Measuring mass changes in single suspended and adherent cells, with applications to personalized medicine in Glioblastoma Multiforme (GBM)

By: Nigel Shijie Chou

B.S. Biomedical Engineering
Duke University, 2009

Submitted to the Department of Biological Engineering
in partial fulfillment of the requirements for the degree of:

Doctorate of Philosophy in Biological Engineering
at the Massachusetts Institute of Technology

June 2017

© Massachusetts Institute of Technology 2017. All rights reserved.

The author hereby grants to MIT permission to reproduce and to distribute publicly paper and electronic copies of this thesis document in whole or in part in any medium now known or hereafter created.

Signature redacted

Signature of Author: _____
Department of Biological Engineering
May 26, 2017

Certified by: _____ Signature redacted _____
Scott R. Manalis
Andrew and Erna Viterbi Professor of Biological Engineering
Thesis Supervisor

Accepted by: _____ Signature redacted _____
Mark Bathe
Associate Professor of Biological Engineering
Graduate Program Chair

ARCHIVES
MASSACHUSETTS INSTITUTE OF TECHNOLOGY
JUL 12 2017
LIBRARIES

Measuring mass changes in single suspended and adherent cells, with applications to personalized medicine in Glioblastoma Multiforme (GBM)

By: Nigel Shijie Chou

Submitted to the Department of Biological engineering on May 26, 2017 in partial fulfillment of the requirements for the degree of Doctorate of Philosophy in Biological Engineering at the Massachusetts Institute of Technology

The author hereby grants to MIT permission to reproduce and to distribute publicly paper and electronic copies of this thesis document in whole or in part in any medium now known or hereafter created.

ABSTRACT

The increased precision offered by developments in suspended microchannel resonator (SMR) technology opens the possibility for measuring small mass changes in cells. Mass accumulation rate (MAR) measurements in single suspended cells over short periods of time have the potential for characterizing heterogeneous collections of tumorigenic cells and serve as a functional marker for the effects of anti-cancer drugs. In this thesis we adapt mass accumulation measurements for use in Glioblastoma Multiforme (GBM) patient-derived cell lines, exploring the heterogeneity between and within patient tumors, and validating the measurement as a predictor of drug susceptibility with response times on the order of 24 to 48 hours using an experimental MDM2 inhibitor.

While MAR measurements can be performed on suspended single cells with high precision, it has not yet been adapted for measuring the growth of adherent cells. We develop a technique to measure mass accumulation in cells adhered to the inner surface of the resonator channel. To overcome challenges inherent in such a measurement, we use infrared imaging and multiple resonant modes to reveal the cell's position in the SMR, and utilize differential measurements from a second cantilever to account for frequency drift.

Thesis Supervisor: Scott R. Manalis
Title: Andrew and Erna Viterbi Professor of Biological Engineering

Acknowledgements

I would like to thank everyone who has helped make this thesis possible.

First, I would like to thank my advisor Scott Manalis for the opportunity to work in his lab. Thank you for your mentorship, guidance and continual support throughout the last 6 years, and especially your concern for my personal development. Thanks for having confidence in me even through my failures, and for correcting me when I needed correcting.

I would also like to thank my thesis committee members Jacquin Niles and Rohit Karnik, who provided valuable advice and support, and helped me see the big picture in my projects.

Thanks to everyone involved in the Glioblastoma project: Keith Ligon, Cecile Maire, Sam Haidar, David Knopf and Mark Stevens. Thanks to Keith for his guidance throughput the project. For Cecile, who was always ready to offer her help and for her confidence in us even at the beginning when nothing was working. Thanks to Samer Haidar who worked many long nights with me during the early stages of developing the drug susceptibility assay. Thanks to David Knopf who performed many of the drug measurements in this thesis. Thanks to Mark who started the collaboration with Cecile and Keith 6 years ago and with whom I worked together on the paper.

Thanks to all in the lab who helped me on various projects. Thanks to the senior graduate students, particularly Sungmin Son and Wesley Weng, who helped me greatly when I first started out in lab. Thanks to Selim Olcum, who was has helped me a lot in all the work I have done in the lab, and who is extremely knowledgeable in any area of engineering. Thanks to Nate Cermak who designed many of the instruments and code behind measurements in this thesis, and who is not only great at troubleshooting but also

explaining what went wrong. Thanks to Joon Ho Kang who worked closely with me on the adherent cell mass measurement project. Thanks to Robert Kimmerling who I spent much time with working on the hydrodynamic traps in the earlier years. Thanks to Teemu Miettinen, who helped me with the adherent cell culture and with whom I have had many good conversations.

Thanks to all my other colleagues: Vivan Hecht for her friendship over the many years of graduate school. To Scott Knudsen, who always reliable and knowledgeable about everything in lab. To Will Grover, Andrea Bryan, Josephine Bagnall, Amneet Gulati, Francisco Delgado, Nicholas Calistri, Bashar Hamza, Arif Cetin, Christopher Chin and Clara Park - it was a joy working with all of you.

Thank you to all those at the Koch and in the BE department: Mariann Murray, Dalia Fares and Susan Jaskela for their help and their hard work in keeping everything running smoothly.

Thank you to my family, my parents, sister and brother-in-law, who believed in me and have always encouraged me and during difficult times.

Thanks to my friends from outside the lab who have supported me though these years, especially from the Graduate Christian Fellowship, particularly Po-ru Loh, Kunle Adeyemo, Ming-Zher and Yukkee Poh, Samuel Perli, Louis Tee, Sze Zheng Yong, Gregory and Hee Yeon Newby, David Kwabi, Peng and Annie Shi, Sam and Grace Elder, Gerald Pho, John Liu and others that are too many to name, and who have demonstrated by example how to be both a committed Christian and a good scientist.

Finally, thanks to my God and Savior Jesus Christ without whom nothing would be possible.

Table of Contents

Chapter 1 Introduction **15**

1.1 Measuring mass changes in live cells **15**

1.2 Measuring buoyant mass of particles using a suspended microchannel resonator (SMR) **17**

1.3 Mass accumulation measurements on mammalian cells **18**

1.4 Interpretation of mass changes in cells **19**

1.5 Critical needs in the treatment and study of Glioblastoma Multiforme (GBM) **20**

1.5.a Benefits of single-cell level characterization in GBM 20

1.5.b Drug susceptibility measurements for personalized medicine in GBM 22

1.6 Patient-derived cell lines for characterization of GBM tumors **23**

1.7 Sensitivity of the MAR measurement of single cells from GBM PDCLs **24**

Chapter 2 Adaptations to the device setup and culture protocol for reliable measurement of GBM PDCLs **27**

2.1 Modifications in system design for use of both low and high quality factor chips **28**

2.2 Adaptations for cell growth on chip **31**

2.3 Protocol for culture, preparation and measurement of GBM PDCL samples **32**

2.3.a Normal bulk-culture protocol for GBM PDCLs 32

2.3.b Specific bulk-culture protocol in preparation MAR measurement 32

2.3.c Channel passivation and reduction of cell clumping 33

2.3.d Dissociation of cells before measurement 34

2.3.e Cell loading and measurement protocol 35

2.3.f Experimental protocol for characterization of GBM PDCLs 37

2.3.g Experimental protocol for drug susceptibility measurements 37

2.3.h Statistical comparison of GBM-PDCL MAR profiles 39

2.3.i Post-measurement chip-cleaning protocol 39

Chapter 3 Alternative techniques for assessing cell viability or growth 41

3.1 The Cell Titer Glo viability assay 42

3.2 Immunofluorescence Assays..... 43

3.2.a KI67..... 44

3.2.b BrdU..... 44

3.2.c Detailed staining protocol 45

3.2.d Results with BT145 over 24 hrs..... 45

3.3 Aggregate cell volume measurement using a Beckman Coulter Multisizer 46

3.4 Single-cell tumorsphere formation assay 49

3.5 Conclusion..... 53

Chapter 4 MAR measurement reveals intra- and inter-tumoral heterogeneity, and predicts drug susceptibility and resistance 55

4.1 Measurement of 7 GBM PDCLs 57

4.1.a Significant MAR heterogeneity observed between and within GBM PDCLs and commercial cell line U87 57

4.1.b Maintenance of MAR heterogeneity across culture passages..... 62

4.2 Drug susceptibility measurements..... 63

4.2.a Desirable characteristics of a drug susceptibility assay 63

4.2.b Predictions of drug susceptibility based on Genetic background of GBM PDCLs 64

4.2.c Results of drug treatments on five GBM-PDCLs 66

4.2.d Validation with Cell Titer Glo viability measurements 70

4.3 Discussion..... 72

4.3.a Applicability of MAR measurement to downstream assays 72

4.3.b Comparison to other functional assays 73

4.3.c Limitations of MAR measurement as a drug susceptibility assay 74

4.4 Conclusion 75

4.5 Appendix: GBM PDCL genetic analysis 77

Chapter 5 Estimation of position-dependent mass changes by combining multiple resonant mode frequency data with image data 79

5.1 Introduction 79

5.2 Theory 81

5.3 Coarse alignment of image and frequency data 85

5.4 Obtaining normalized position information from image frames 87

5.5 Fine alignment of image and frequency data 89

5.6 Results of mass estimation 92

5.7 Possible causes of erroneous mass estimate 96

5.8 Conclusion 97

Chapter 6 Towards measurement of mass accumulation in adherent mammalian cells 99

6.1 Introduction 99

6.2 Suspended particle measurements vs adherent measurements in an SMR 101

6.3 Overcoming engineering challenges inherent to measuring adherent cells 102

6.3.a Cell position uncertainty 102

6.3.b Maintaining cell viability 103

6.3.c Frequency drift 104

6.4 Results and discussion 108

6.5 Future directions 110

6.6 Conclusion 112

6.7 Appendix 1: Alternate mass trajectory data **113**

6.8 Appendix 2: Frequency noise compared to drift over time **114**

6.9 Appendix 3: Manual identification of cell boundaries **115**

Bibliography **117**

List of Figures

Figure 1-1: Heterogeneity in cultured single GBM cells 21

Figure 1-2: Mass accumulation measurement schematic 25

Figure 2-1: Chip and clamp setup schematic 30

Figure 2-2: Example measurement with BT159 38

Figure 3-1: Techniques for measuring cell viability and proliferation 48

Figure 3-2: Cell isolation in SMR vs bulk culture 51

Figure 3-3: Cell isolation: positive vs negative MARs 53

Figure 4-1: MAR vs mass profiles for all cell lines 59

Figure 4-2: Staining and percentage of cells positive for KI67 61

Figure 4-3: MAR per unit mass for all cell lines separated by passage 62

Figure 4-4: P53 Signaling pathway and relevant PDCL mutations 65

Figure 4-5: Results of MAR drug-susceptibility experiments 67

Figure 4-6: MAR vs mass in response to drug. 69

Figure 4-7: IC50s for cell lines using Cell titer glo 71

Figure 5-1: General schematic for multimode mass estimation with imaging 80

Figure 5-2: Simple model of cell dimensions 82

Figure 5-3: Triggering using first mode peaks 86

Figure 5-4: Alignment between modes 88

Figure 5-5: Estimation of mass pre-constriction and time alignment 91

Figure 5-6: Typical mass estimate of U2OS cell 93

Figure 5-7: Frequency deviation shown as a function of position 94

Figure 5-8: Representative plot of frequency deviation in a U2OS cell. 95

Figure 6-1: Measurement cycle illustration 103

Figure 6-2: Multi-cantilever chip design repurposed for reference measurement .105

Figure 6-3: Differential measurement in second resonant mode 107

Figure 6-4: Differential measurement in first resonant mode.....107

Figure 6-5: Raw data from measurement of Hela cell over 2 generations.....108

Figure 6-6: Mass estimate of Hela cell grown for 2 generations 109

Figure 6-7 Tweaks in chip design for improved adherent cell measurement.....111

Figure 6-8: Alternative mass estimate trajectory for a cell 113

Figure 6-9: Frequency noise vs long term drift 114

Figure 6-10: Procedure for drawing cell boundaries in matlab code 115

Chapter 1

Introduction

1.1 Measuring mass changes in live cells

Over the last decades, significant advances have been made in the use of micro and nano-mechanical resonators to analyze biological samples, taking advantage of their extraordinary sensitivity and mass resolution [1]. The invention of vacuum-packaged resonators encompassing fluidic channels have opened up new possibilities for measuring living biological samples such as bacteria, yeast and mammalian cells with the ability for cells to remain immersed in culture media during measurement, without sacrificing the characteristic high quality factors of resonators operating in vacuum ([2],[3],[4],[5]).

Such resonators, known as suspended microchannel resonators (SMRs), can not only determine the mass of individual cells, but have sufficient measurement precision to resolve small changes in cell mass. An application that has the greatest potential is charting the change in cell mass over time, reflecting the accumulation or loss of mass of the cell over time. This type of measurement has been shown in tracking single mouse lymphoblasts over multiple cell cycles to study cell cycle dynamics [6]. In this thesis we show that similar measurements of single cell mass accumulation rates, made over short periods of time on the order of minutes and on many cells, has utility as an assay for drug susceptibility in cancer cells. We demonstrate such measurements in patient-derived cell lines of Glioblastoma Multifome (GBM), a deadly brain carcinoma that can benefit greatly from rapid drug testing for patient diagnosis. In addition, we show how our measurements reveal cell-to-cell variability both between and within GBM tumors, potentially furthering our understanding of this highly heterogeneous cancer.

In the final chapters, we explore ways of measuring mass changes in cells that incorporate information on the position of the cell on the resonator. First, we outline our attempts to measure small short-term changes in buoyant masses of cells passing through a constriction. We then show how we can adapt the use of SMRs to measure mass accumulation in adherent mammalian cells growing on the inner surface of the resonator channel, using both position and frequency information together with differential sensing, and show the first measurements of adherent cells grown in an SMR.

1.2 Measuring buoyant mass of particles using a suspended microchannel resonator (SMR)

The design and operation of suspended microchannel resonators (SMRs) have been described previously [1, 4, 6], and will be summarized here for the reader's benefit. An SMR is a microfabricated cantilever-based mass sensor. The central feature of each device is a fluid-filled cantilever suspended in a vacuum cavity. The hollow channel of the cantilever is connected to a series of channels etched in the silicon that eventually lead to entry ports on the surface of the chip where measurement samples can be introduced.

The basic measurement principle is as follows: the cantilever's resonance frequency depends on the mass distribution along its length. The presence of a particle with density different from the fluid density in the cantilever's channel results in a change in resonance frequency relative to the same cantilever containing only fluid. The change in mass, given by the excess mass of the particle over the mass of the displaced fluid (referred to as buoyant mass), can be shown vary approximately linearly with the change in resonant frequency as long as it is much smaller than the mass of the cantilever [2]. This allows direct calibration to be carried out between the frequency change observed and the buoyant mass of the cell. For simplicity, buoyant mass will be referred to as mass in the rest of this thesis.

1.3 Mass accumulation measurements on mammalian cells

Accumulation of mass of the cell can be estimated by making repeated mass measurements over time. To do so, we carefully control pressures at the entry ports of the chip using high-precision pressure regulators, holding a cell stationary in fluidic channels close to the cantilever, then moving the cell across the cantilever at regular intervals to make repeated mass measurements (**Figure 1-2**). This technique has been used to follow a single cell and its progeny over multiple cell cycles in a study of cell cycle dynamics in the highly uniform mouse lymphoblast cell line L1210. [6].

We can take advantage of the higher measurement sensitivity of the SMR achieved by improvements in measurement techniques, such as utilizing the second resonant mode of the cantilever [8], to measure mass accumulation in cells on shorter time scales on the order of minutes. We are able to resolve the instantaneous rate of mass accumulation for a single cell in approximately 10 to 15 minutes. The single-cell mass versus time data can be linearly fitted to determine mass accumulation rates (MAR) given in pg/hr. Measurements of MAR over this timescale have a limit of detection in the range of 0.3 pg per hr when the cell is weighed at sufficiently short intervals of 30 - 90 seconds.

1.4 Interpretation of mass changes in cells

What is the relevance of making precise measurements of mass accumulation in cells? In particular, what information can be obtained by capturing 'snap-shots' of mass accumulation in cells over periods of 10-15 minutes? Consider that at any point in time a cell is taking up nutrients and secreting waste products. If uptake is not equal to secretion, the cell must be changing its mass. A common situation is that of an actively growing and dividing cell. Such a cell will need to take up large quantities of nutrients and raw material for DNA replication and protein synthesis, and will need to add additional material to its various components and organelles in preparation for division into daughter cells. Hence an increase in mass of a cell is likely to be associated with active cell growth, and a large positive mass accumulation rate may indicate an actively growing cell.

However, not all cells are actively growing and there are situations in which a cell may be maintaining or losing its mass due to the present state of the cell and as it responds to changes in its environment. However, interpretation of such a measurement is not always clear. For example, a cell undergoing apoptosis is expected to be decreasing in mass, yet observing a decrease in mass alone need not necessarily imply apoptosis and may involve temporary size regulation or adaptation of a cell for a different role. The implications of such mass changes will be discussed further later in this thesis.

1.5 Critical needs in the treatment and study of Glioblastoma Multiforme (GBM)

Glioblastoma Multiforme (GBM) is the most common malignant brain tumor. It is an aggressive and deadly cancer that is resistant to most treatments and has a high recurrence rate. The typical survival time of patients with treatment is 15 months [9, 10], while the median time to recurrence after standard-of-care treatment is a mere 7 months. The current standard treatment of GBM patients is surgical resection of the tumor mass when possible, followed by radiotherapy and concomitant adjuvant chemotherapy with Temozolomide [11, 12].

Since GBM is diagnosed only at a late stage when the tumor has become large enough to produce symptoms, its origin and development is poorly understood. The last major advance in GBM treatment was over a decade ago in 2005, when the addition of Temozolomide to radiotherapy was shown to improve the 2 year survival rate from 10% to 27% [11]. While improved understanding of underlying genetics has revealed possible drug targets [13], there have not been any successful clinical trials to date.

1.5.a Benefits of single-cell level characterization in GBM

One of the main challenges in the study and treatment of GBM is the heterogeneity present within each tumor, which actually consists of a variety of cell-types that are genetically and morphologically distinct.

The reason for the high recurrence rate is that a small subpopulation of tumor cells can repopulate the tumor even after most of the cells are removed by surgical resection and the patient has undergone subsequent radiotherapy or chemotherapy.

In addition, GBM tumors vary widely between patients. Although there have been attempts to classify GBMs genetically into sub-types ([14],[15]), such subdivisions are controversial and not well defined. This histological and genetic heterogeneity poses challenges for the development of targeted therapies, which existing population-level experiments often mask. Hence, measurements on the single-cell level have the potential to contribute significantly to our understanding of GBM. The MAR measurement, performed on single cells, has the potential to reveal the heterogeneity within and between patient tumors, and given enough patient data may eventually be used to make correlations with patient outcome and genetic markers.

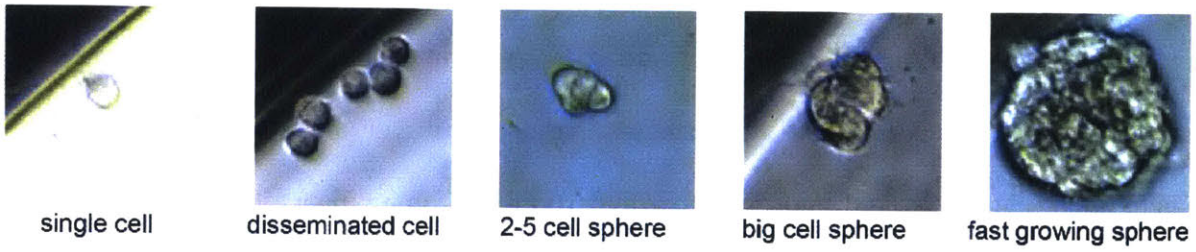

Figure 1-1: Heterogeneity in cultured single GBM cells
Bright field images of single-cells dissociated from a GBM PDCL in 92-well plates, after a culture period of 2 weeks. A fraction of the cells are capable of growing into tumorspheres, but significant heterogeneity is observed even in the size and morphology of these spheres. Images from Cecile Maire

1.5.b Drug susceptibility measurements for personalized medicine in GBM

Due to the short survival times of patients and high heterogeneity between GBM tumors, a personalized medicine approach can have a significant impact for patients suffering from GBM. The MAR measurement has the potential to be very useful since it is a more direct measurement of the proliferation characteristics of cells compared to most molecular or genetic tools. In addition, as we will show later in this thesis, the MAR has the ability to detect drug effects as early 13-24 hours after introduction of the drug. This is likely because decreases in MAR occur before the cell has reached a point in apoptosis (typically membrane permeabilization) that can be detected by viability assays. With improvements in throughput and reliability, the MAR has the potential to be a more sensitive and rapid technique to assess the susceptibility of a particular patient tumor to a drug.

Such personalized measurements of drug effectiveness have clear benefits to patient survival by allowing for rapid testing of drugs to determine what drug or drug combination is likely to work for a particular patient. However, there are other important benefits of personalized drug testing, particularly in improving the well-being of the patient. Since most cancer therapies have detrimental side-effects, being able to predict beforehand if a drug will be effective can allow doctors to avoid administering a costly drug that would have no effect on the patient, saving the patient great cost and discomfort.

1.6 Patient-derived cell lines for characterization of GBM tumors

Model cell lines used in cancer research have traditionally involved cells that have been selected for their ability to survive indefinitely in culture, and would have been cultured over a large number of passages before being used. As cells are cultured over extended time periods, they tend to shift their characteristics due to selection pressures in the specific culture environments. Hence it is unclear how closely these model cell lines resemble primary tumor cells. In addition, due to the heterogeneity present in Glioblastoma, it is necessary to be able to model tumors from different patients in order to fully understand all aspects of this disease.

To address this lack of suitable models, the Ligon group at the Dana Farber Cancer Institute (DFCI) has developed a way to culture GBM cells derived from patient tumor samples which genetically and morphologically recapitulate the primary tumor, and retain these properties for up to 20 generations in culture. The main advantage of such patient derived cell lines (PDCLs) compared to conventional cell lines is the potential of such models to preserve aspects of the phenotypic and genomic heterogeneity seen in patient tumors. To maintain the patient tumor derived cells in culture, they have adapted neural stem-cell culture techniques, in which the cells grow as dense clumps of cells known as neurospheres or tumorspheres suspended in culture media. The 3D sphere-like structure of such tumorspheres is theorized to more closely resemble the tumor environment and organization compared to culture on a flat surface.

The culture protocol will be explained in more detail in the next chapter. For the purposes of this thesis, we will refer to such cultures as patient-derived cell lines, or PDCLs, since each culture is derived from a single patient sample. GBM-PDCLs currently provide the best available model system for studying the molecular and genetic characteristics of GBM tumors, as well as for assaying the effects of novel drugs and treatments.

1.7 Sensitivity of the MAR measurement of single cells from GBM PDCLs

In the first half of this thesis, we will show how we adapted the MAR measurement for use on these GBM PDCLs. To give an idea of the precision of the measurement in this application, the magnitude of MARs measured in single-cells from GBM PDCLs are on the order 10s of pg/s. As an illustration of the sensitivity of the system, mass accumulation rates on the order of picograms would correspond to an increase in cell diameter on the order of 10nm. Such sensitivity cannot currently be achieved even in high-resolution optical measurements.

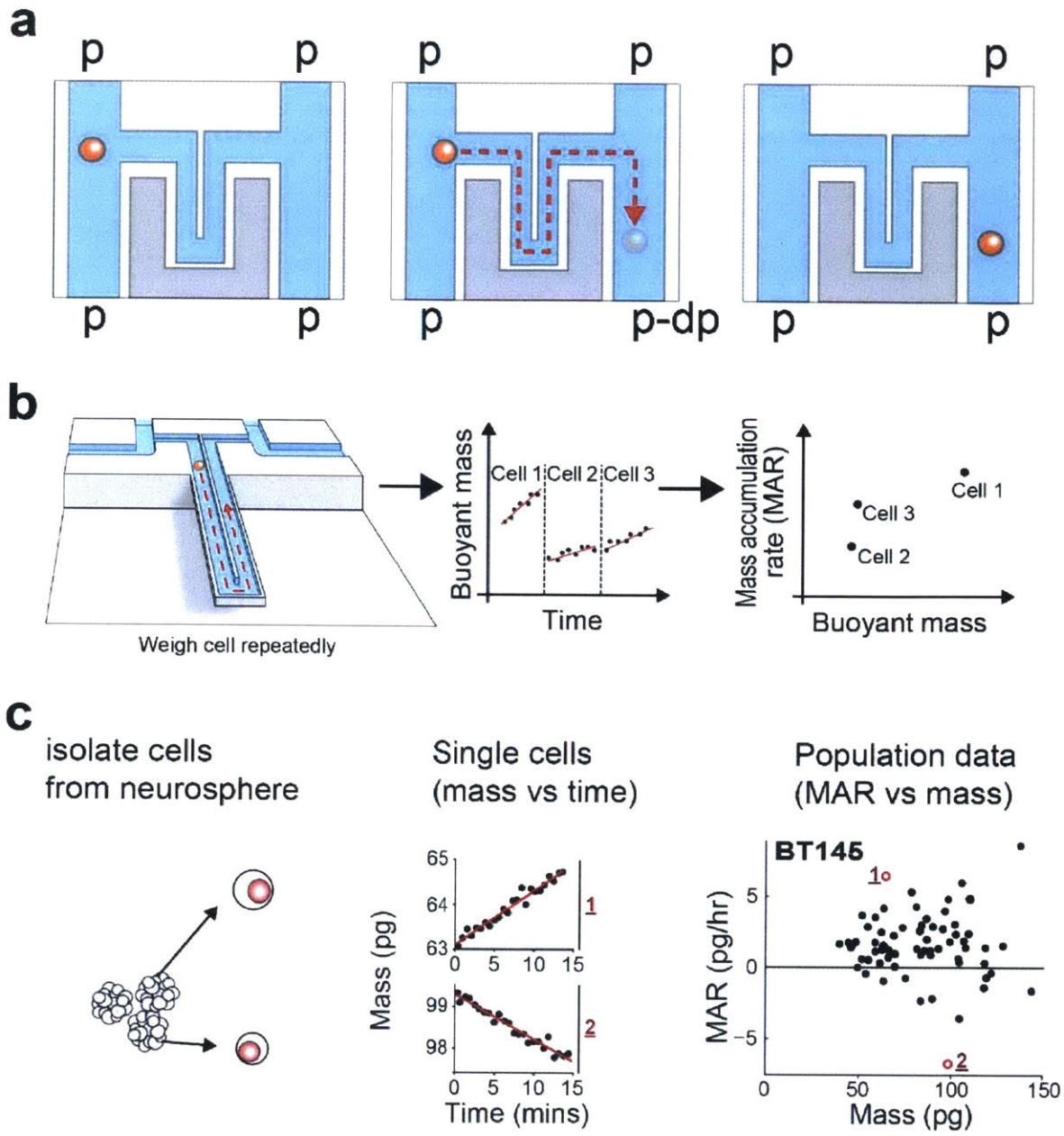

Figure 1-2: Mass accumulation measurement schematic
(a) Simplified schematic showing how a cell can be held stationary in a side channel by carefully matching pressures (p). When making a measurement, the cell can be moved across the cantilever by lowering the pressure in one of the 4 entry ports (p-dp in the lower right port). Once in the opposite channel, the cell can be returned to the left channel in a similar manner. (P represents a fixed pressure while dP represents a step change in pressure that can be varied to control the speed of the cell) (b) Representative schematic showing measurements of 3 cells (c) Actual data showing how measurement of single cells isolated from GBM neurospheres can be used to build up profiles of MAR and mass over a population of cells.

Chapter 2

Adaptations to the device setup and culture protocol for reliable measurement of GBM PDCLs

Previously, mass accumulation measurements have been demonstrated in lymphoid cells [6], bacteria and yeast [4],[5]. In this chapter we explain adaptions to the general technique that allow us to reliably measure single cells dissociated from GBM PDCLs, describe a number of modifications made to the measurement system to improve robustness of the measurement, and outline culture protocols that improve the reliability of cell capture and manipulation during an experiment.

2.1 Modifications in system design for use of both low and high quality factor chips

The design of the measurement system was modified to effectively utilize low quality-factor (Q) chips. The modifications are designed to reduce system noise and improve chip actuation. They allow previously unusable chips to be utilized for MAR measurements, and may enable future chip designs with a simplified fabrication process that can be manufactured more quickly.

Firstly, a Field Programmable Grid Array (FPGA) is used for signal acquisition and frequency generation in place of discrete electronics, helping to reduce noise levels. With this setup, a high-current voltage amplifier circuit is still required to drive the cantilever to a sufficiently high amplitude.

In order to achieve low noise on a resonant system with low Q, the driving force has to be increased significantly. Previously, the actuation force was delivered by a multilayered piezoelectric crystal embedded in the clamp holding the chip. The chip would be pressed tightly onto the clamp to ensure good contact. Exerting high pressure on the chip by over-tightening the set-screws is often required for a good physical connection to allow effective actuation. However, contact is typically not optimal and excessive force may result in damage or breaking of the chip.

To increase the actuation force on the cantilever to sufficiency high levels without damaging it, we bonded the chip directly to the piezoelectric crystal with a thin layer of hard epoxy to maximize coupling between crystal and chip. In addition, existing piezocrystals were replaced by larger 10mm x 10mm single-layered piezocrystals in order to maximize contact area to the chip. In addition, single-layered piezocrystals are easier to drive and have smaller current requirements. The clamp holding the chip was modified accordingly to hold the piezocrystal and its electrical connections (**Figure 2-1**).

The main disadvantage of this modification is that a piezocrystal is required for every chip, since chips are bonded permanently to the piezocrystal. Nonetheless, this is a practical solution since single-layered piezocrystals can be obtained relatively cheaply, and cost significantly less than the chips themselves. In addition, a microfluidic chip without any major defects typically has a useful lifetime of at least 6 months under heavy use. A second potential limitation is that bonding the piezocrystal directly to the back of the chip blocks optical access to the chip from the back-side. Because of this constraint, the optical system was set-up such that both the laser spot for frequency readout and the imaging optics are directed at the top surface of the chip. A short-pass or notch filter was added to the imaging optics to eliminate the laser light at 635nm, allowing for a reasonably good image of the cantilever and the surrounding channels.

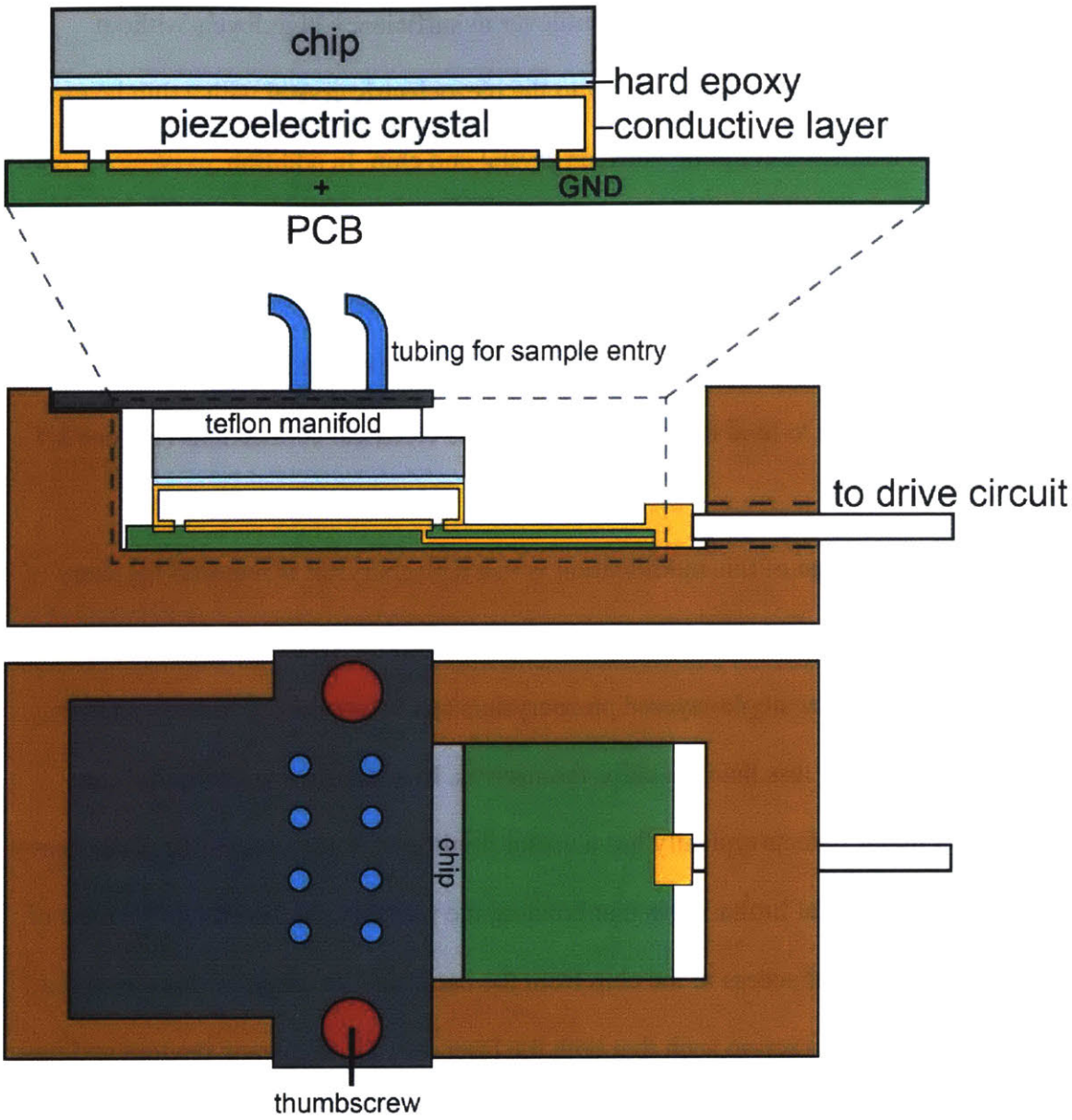

Figure 2-1: Chip and clamp setup schematic
Schematic of a chip directly attached to the piezoelectric crystal and PCB. A schematic of the full clamp setup is also shown. The clamp and face-plate are unchanged, but the PCB and electrical connections have been modified. Thumbscrews are used to ensure a secure fluidic seal between tubing and chip, preventing leakage of sample onto the PCB. An embedded channel in the copper clamp (not shown) is connected to a continuous-flow water bath set at 37° Celsius to keep the entire system an even temperature.

With this setup, the low Q chips showed baseline noise levels within a factor of 2 of that of high-Q chips used for earlier measurements. We also tested if the higher actuation forces would be detrimental to cell viability and growth by performing MAR measurements on a number of L1210 cells, comparing this to similar data obtained from control experiments done on high-Q chips. Since the MAR measurements did not differ significantly between the high-Q and low-Q chips, we concluded that cell-viability was not affected by the higher actuation forces.

2.2 Adaptations for cell growth on chip

The cell-measurement setup was modified to mimic conditions in a cell-culture incubator, ensuring optimal conditions for maintaining cell viability during a measurement. The microfluidic chip was mounted on a copper clamp (**Figure 2-1**) connected to a temperature-controlled water bath at 37°C. The vial containing the cell sample was placed on a hot-plate set at 37°C during measurement, and the sample vial was replaced with fresh cells from the culture flask after 5-6 measurements or approximately 1-2 hrs. Both sample and media vials were pressurized using 5% CO_2 to ensure appropriate pH buffering in the media surrounding the cells throughout the experiment.

2.3 Protocol for culture, preparation and measurement of GBM PDCL samples

2.3.a Normal bulk-culture protocol for GBM PDCLs

Following the protocol used in the Ligon lab, the GBM PDCLs were grown in NeuroCult NS-A proliferation media (Miltenyi) supplemented with 2 μg/ml Heparin, 20 ng/ml human epidermal growth factor (EGF), 10 ng/ml human bFGF in ultra-low attachment coated flasks (Corning, Cat#3814), which are kept in a 37°C, 5% CO_2, and humidified incubator. When passaged, the neurospheres were dissociated into single-cells by enzyme treatment and repeated pipetting, then re-seeded in fresh media.

2.3.b Specific bulk-culture protocol in preparation MAR measurement

Following the above protocol, the GBM PDCLs were cultured in low-attachment flasks using Neuro-cult media, with the EGF and bFGF added fresh at each passage. Passage times varied from 4 days to 2 weeks depending of the specific PDCL. Although passage times for cultures to grow to confluence are reasonably reproducible, care was taken to ensure that the neurospheres did not grow so large that their centers became necrotic. Cultures were passaged early if such conditions were observed.

When a MAR measurement experiment is conducted, cells are obtained from cultures that were passaged 1-2 days early. This change in protocol is based on the observation that cells dissociated from highly confluent cultures tend to be stickier after dissociation making them more difficult to handle fluidically on chip.

2.3.c Channel passivation and reduction of cell clumping

Due to the variablity in shape and size of GBMs and their propensity for sticking to each other and the surfaces of culture vessels, optimizing sample preparation is essential for making reliable measurements of GBMs without compromising the measurement device. To prevent cells from sticking to walls, we experimented with various methods of channel surface passivation. One technique attempted was to coat the channels by covalent passivation with PEG-silanes, which we theorized would increase the hydrophobicity of the channel walls and reduce sticking to highly charged cell surfaces. However, this channel passivation technique provided only minimal reduction in cell sticking, and was extremely time consuming when accounting for both the passivation step in which the PEG-silane is left in the channel and allowed to adhere to channel walls, and subsequent washing steps which required multiple hours of flushing with isopropanol and deinonized water to ensure that the channels could again be conducive for cell growth. In addition, it became apparent that cells sticking to each other to form clumps was more of an issue than the phenomenon of cells sticking directly to channel walls.

Ultimately, we found that the most effective protocol was to add Poly L-Lysine/ Polyethylene Glycol (PLL-PEG) directly to the culture medium. Polyethylene Glycol is hydrophobic and hence relatively inert to biological material, while Poly L-Lysine has a high concentration of positive charge that allows it to bind to the silicon surfaces of the channel. We theorize that the effectiveness of this technique is partly due to the PLL binding to negatively charged molecules on the cell surface, reducing sticking both between cells and between cells and channel walls.

We tested the effect of PLL-PEG by adding them at various concentrations to cultures of BT145 PDCLs, and found that neither doubling times nor morphology of the neurospheres changed significantly, showing that the addition of PLL-PEG did not negatively affect cell growth. Through such testing, we selected a ratio of 10μl of PLL-PEG per ml of culture media for use in MAR measurements.

2.3.d Dissociation of cells before measurement

A second important factor is the process by which cells are dissociated before measurement. The dissociation of cultured neurospheres into single cells during regular cell passaging involves the addition of a proteolytic enzyme to break up cell adhesion molecules, followed by repeated mechanical shear using a pipette tip to break the tumorspheres into individual cells.

Such perturbations affect the condition of cells to some extent and may temporarily hinder growth, resulting in sub-optimal measurements if the cells are measured too soon after dissociation. However, if cells are left for too long after dissociation, they start to clump together to re-form spheres which may be too large for the channels and may clog the channels in the device. Hence, we aimed to optimize time after dissociation during which cells were measured. However, due to relatively low throughput of the MAR measurement of 3 cells/hr, we started measuring the cells immediately after dissociation and stopped after at most 8 hrs, when significant clumping begins to occur.

We determined that the optimal dissociation protocol was to use Accutase(R) solution (Sigma-Aldrich), an enzyme mixture designed to be gentler than trypsin, for 5-8 min to loosen the neurospheres, followed by 4-5 rounds of very gentle mechanical pipetting. Our attempts to eliminate enzyme mixtures and use only mechanical dissociation resulted in sticky cells that were difficult to handle fluidically on-chip. Hence we recommend use of gentle enzymatic degradation for cell preparation over mechanical dissociation as the most suitable method for preparing cells for MAR measurement.

2.3.e Cell loading and measurement protocol

For measurement in the SMR, cells were suspended in the same NeuroCult media used for bulk-culture. The cell sample was diluted to 70-100 cells/ml, and PLL-PEG was added at 10 μl/ml as described earlier to reduce cell-clumping and sticking to microchannel walls.

Each cell was measured at 25-35 second intervals by passing it across the cantilever using slight changes in pressure applied alternatively to the left or right downstream ports (**Figure 1-2**). Between measurements, cells were held static in the bypass channels by equalizing all port pressures, as described earlier. Each cell was measured for 15 min each (approximately 30 measurements) before being flushed down the right bypass channel. Subsequently, a new cell was drawn up from the sample vial via the left bypass channel.

Small particles such as debris from dead cells are excluded automatically by applying a minimum peak-height threshold, set to only allow larger particles (cells or clumps of cells) to be measured. In a subset of cell lines (BT179 and BT320), we encountered cells that are too large or were clumped together due to imperfect dissociation. When detected, these cells were manually excluded from measurement by flushing the bypass channels to clear the cell from the chip. In a small number cell lines (BT484) cells had a tendency to stick to channel walls despite the preventative measures described in the previous section. In the rare cases when a cell gets stuck to a channel wall, we were able to continue measurement by gently tapping the sample vial or connecting tubing to dislodge the cell.

2.3.f Experimental protocol for characterization of GBM PDCLs

We measured MARs of single cells derived from tumorspheres in PDCL culture, obtaining mass trajectories as described. Each measurement was conducted over a period of 6 to 8 hrs immediately after dissociation of neurospheres into single cells. We measured between 15 and 25 cells in each experiment, and made 3 biological replicates for each PDCL. An example of the measurements taken, as well as a representative mass trace, is shown for one cell line (BT159) in **Figure 2-2**.

2.3.g Experimental protocol for drug susceptibility measurements

In cases when drug treatment was being tested, GBM-PDCLs were seeded into parallel cultures and treated with 1 μM of drug (MDM2 inhibitor RG7112), or DMSO. At each time point, one parallel culture was dissociated and immediately resuspended in drug media, and the remaining parallel cultures were resuspended in fresh media with new drug. The dissociated cell suspensions were kept in drugged media during the measurements.

We performed the maximal number of measurements possible for the duration of each time point (between 10 and 20), but measurement throughput was limited by practical limitations such as ease of handling of particular cell lines and increased sticking of cells to channel walls after extended drug treatment.

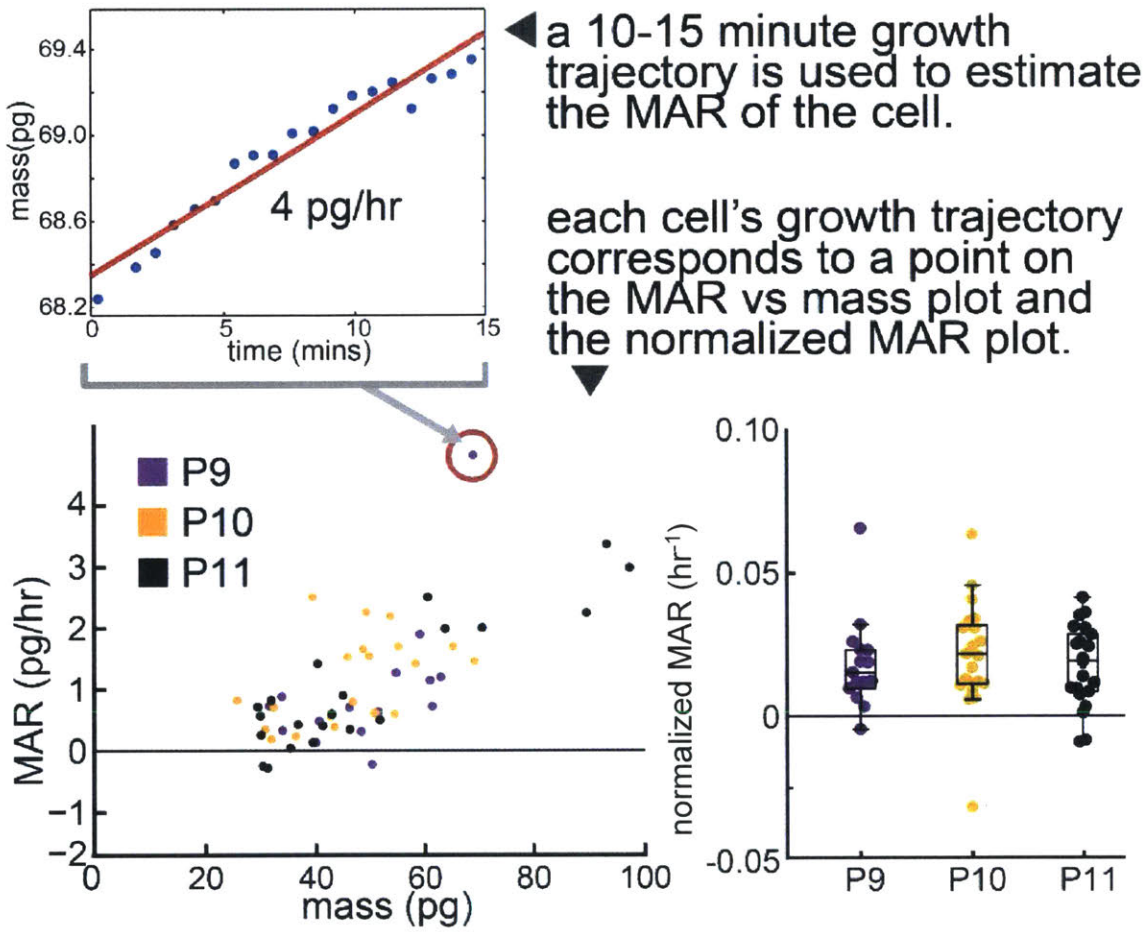

Figure 2-2: Example measurement with BT159
Plots of measurements from a single cell line BT159. An example of a single cell mass trace is shown, corresponding to a point on the MAR vs mass plot shown by the red circle. On the MAR vs Mass plot, measurements are color coded according to passage. The corresponding normalized MAR plot over 3 passages is shown on bottom right. The normalized MAR, or MAR per unit mass representation is used to better visualize changes between successive measurements across culture passages.

2.3.h Statistical comparison of GBM-PDCL MAR profiles

To compare different biological replicates or time points in a drug-susceptibility experiment, we used the Mann-Whitney U test, a nonparametric test of the null-hypothesis that a randomly selected sample from one distribution (e.g. a time-point measurement or control) would be less than or greater than a randomly selected sample from a second distribution. It is similar to the student's t-test with the key difference that a Gaussian distribution is not assumed. We chose this test over the t-test because we could not assume that MARs in a heterogeneous GBM-PDCL follow a Gaussian distribution.

2.3.i Post-measurement chip-cleaning protocol

After every experiment, channels in the chip were flushed with Accutase (the same enzyme solution used for cell dissociation) for a minimum of 20 min to digest and remove any cell debris that may have accumulated on the channel walls. The channels are then flushed with deionized water for 2 mins, followed by 70% isopropanol. This procedure was sufficient to keep channels free of debris after most experiments. In the rare event that a large clog occurs in one of the channels and more severe cleaning was required, we flushed channels with a detergent (10% Micro90 solution from Sigma Aldrich) for up to 30 min followed by deionized water for up to 1 hr. When the system is not in use, all channels and connecting tubing were kept immersed in a 70% isopropanol solution.

Chapter 3

Alternative techniques for assessing cell viability or growth

There are a number of methods of assessing viability and proliferation in GBM PDCLs and tumors, ranging from chemiluminescent methods that work on cell suspensions to immunohistochemical markers that enable identification of proliferating cells in histological sections or fixed cells. These techniques have a long history of use for characterization of GBM tumors as well as in other cancers. We describe these techniques and discuss their ability to detect proliferation or increases in biomass over short time frames on the order of hours, and how they compare to the MAR assay.

We outline a number of such methods in this chapter, including the commonly used Cell Titer Glo viability assay and immunohistochemistry with KI67 and BrdU, two markers of proliferation and DNA synthesis respectively that are used on both GBM tumor sections and PDCLs. In addition, we describe a method of estimating changes in aggregate cell volume of a culture using a Beckmann Coulter Counter. We applied these methods to measure cell proliferation on short time scales of hours, using a relatively fast growing GBM-PDCL (BT145). We also describe a single-cell tumorsphere formation assay, which we used to compare single cells isolated after MAR measurement to single cells isolated from bulk culture, showing that the MAR technique does not have detrimental effects on the cells' proliferation capacity.

3.1 The Cell Titer Glo viability assay

In GBM research, the most commonly used method to assess viability, other than cell counting, is the Cell Titer Glo (Promega) assay. The Cell Titer Glo assay is a chemiluminescence assay that quantitates the levels of ATP in a sample. Since ATP is present in metabolically active cells, the assay can be used as a general measure of viability. The assay is simple to perform, requiring a single reagent, no washing steps, and has a relatively quick response time of 10 min. Typically, we found that a minimum of 100 cells per well are required to obtain a reproducible result although for the following experiments we used cell numbers on the order of 1000s of cells to obtain more reliable data.

We tested the Cell Titer Glo assay on BT145 for short time scales. We plated cells at 2000 cells/well in 96 well plates with ultra-low coating (Corning) and made measurements in triplicate every 2 hours up to 8 hrs and at 24 hrs. The results are shown in **Figure 3-1** (a). We observed an approximate 30% increase at 8 hrs and an increase of about 60% from the initial luminescence value at 24 hrs. We also performed an additional 6 day experiment with measurements taken each day, extrapolating a doubling time of 1.6 days. Based on the doubling time we measured, we suspect that the rapid 30% increase of proliferation that we observed between 6 and 8 hours is most likely an artifact based on the overall growth expected in 6 days. Hence we concluded that the Cell Titer Glo assay was not sensitive enough to reliably measure a change in cell proliferation on a 2 to 8 hr time frame.

3.2 Immunofluorescence Assays

Immunostaining of tumors and cells extracted from PDCLs for cell cycle markers such as Ki67 and BrdU can provide valuable information on fractions of cells that are proliferating or replicating [16], and can later be correlated with MAR measurements. The immunofluorescence assays described below and in subsequent chapters were performed at the Ligon lab in DFCI by Cecile Maire.

3.2.a KI67

KI67 is commonly used as a marker for determining the growth fraction of a given cell population, since the KI-67 protein is associated with cell proliferation and is present during all active phases of the cell cycle (G1, S, G2 and mitosis) but absent from cells in the G0 phase [17].

This marker is particularly helpful in analyzing GBM tumors and PDCLs since they are known to have a subpopulation of cells that are quiescent and would be negative for KI67. Hence KI67 can be used to find the percentage of proliferating cells. As we will show in subsequent chapters, KI67 immunostaining of PDCLs and tumors can provide information on the heterogeneity of the PDCL which can be compared to heterogeneity observed in MAR measurements on the same PDCL.

3.2.b BrdU

BrdU, or Bromodeoxyuridine (5-bromo-2'-deoxyuridine), a nonradioactive analog of thymidine, is a marker of DNA synthesis. It is commonly used as a marker for replicating cells, and has shown promise as a clinical indicator of tumor progression in Astrocytic tumors [18]. BrdU added to culture is incorporated into the newly synthesized DNA of replicating cells during S phase, and substitutes for thymidine. Antibodies specific for BrdU can then be used to detect the incorporated chemical after fixation of the cells followed by denaturation of DNA.

3.2.c Detailed staining protocol

The tumorspheres were fixed in 4% paraformaldehyde and embedded in paraffin after a dehydration cycle. Five micron sections were then deparaffinized and subjected to antigen retrieval in 10mM citrate buffer for 20 min in a steamer. After a 10min incubation in HRP blocking solution, the sections were incubated overnight at 4°C with the following primary antibodies: KI67 (1:100; Vector Labs) and BrdU (1:100, BD/Pharmingen). After washing in PBST, the slides were incubated in secondary antibodies for 1hr at room temperature with anti-mouse alexa 566 (1:1000, Molecular probe) or anti-rabbit alexa 488 (1:1000, Molecular probe). The sections were counterstained with bisbenzimide 33342 (sigma-aldrich) and mounted in fluoromount medium (Southern technology). Prior to fixation, the neurospheres were grown with 10mM of BrdU in the media for 2, 4, 6, 8 and 24 hrs.

3.2.d Results with BT145 over 24 hrs

As shown in **Figure 3-1**(c), the KI67 positive fraction remained constant over all time points, showing that the fraction of proliferating cells did not change significantly after dissociation. Hence, KI67 is useful as a general assay of proliferation fraction but is less helpful for capturing short term culture dynamics. BrdU showed an increase from 0–2 hrs which is sustained up to 8 hrs and rose to 80% after 24 hrs. This assay may useful for showing the general fraction of cells undergoing replication shortly after dissociation but does not have good time resolution on the order of hours since it showed very similar levels in all early time points.

3.3 Aggregate cell volume measurement using a Beckman Coulter Multisizer

We also developed a cell volume measurement using Beckman Coulter Multisizer 4 coulter counter. The Coulter counter measures the change in impedance of particles as they pass through an aperture. The impedance measured is proportional to the volume of the particle, providing a direct readout of cell volume and cell number.

Although such equipment is rarely used in GBM research, we chose to make this measurement because it provides an alternative assay of a physical parameter of the cell - cell volume, as opposed to the commonly used techniques described earlier which rely on quantification of molecular species. Furthermore, unlike the MAR measurement that uses highly specialized microfluidic chips and control systems, this assay makes use of commercially available laboratory equipment.

This assay differs from the typical usage of the coulter counter, which is more commonly used to find averages or variances in individual cell volumes. To obtain a more appropriate metric for the overall biomass of cells in culture, volumes of all cells measured from a fixed volume of culture sample (100 μl) were summed, to obtain an aggregated volume measurement which we refer to as 'summed volume'. We aimed to use summed volume measurement to confirm that there is indeed increase in biomass in the culture over time, and to explore how long it will take to measure such a change.

Cells were dissociated thoroughly to ensure even distribution and prevent clogging of the instrument. 100 μl of cell sample from each time point was diluted into 10 ml of electrolyte solution (PBS or isoton solution provided by Beckman Coulter), and 2 ml of the mixture was drawn through a 100 μm aperture into the instrument. All measurements were done in triplicate and averaged. The same procedure was performed with 10 μm beads at 200,000 per ml as a control (shown in green on **Figure 3-1**(b)).

As shown in the summed volume plot (**Figure 3-1**(b)), we did not observe a significant change in summed volume measurement over the period of 2-6 hrs, but did observe an increase of approximately 40-50% after a period of 24 hours. We conclude that this method of assessing physical characteristics of cells is not sufficiently sensitive on a short time scale on the order of hours, but that given enough time some increase in aggregate cell volume can be observed.

This experiment was performed in conjunction with a MAR measurement, on the same cells dissociated from a BT145 culture flask at passage 11. As seen in **Figure 3-1**(d), the MAR measurement displayed significant numbers of cells with positive MARs over an 8 hr experiment, showing better ability to capture information on the cells over the same time scale compared to the summed volume measurement.

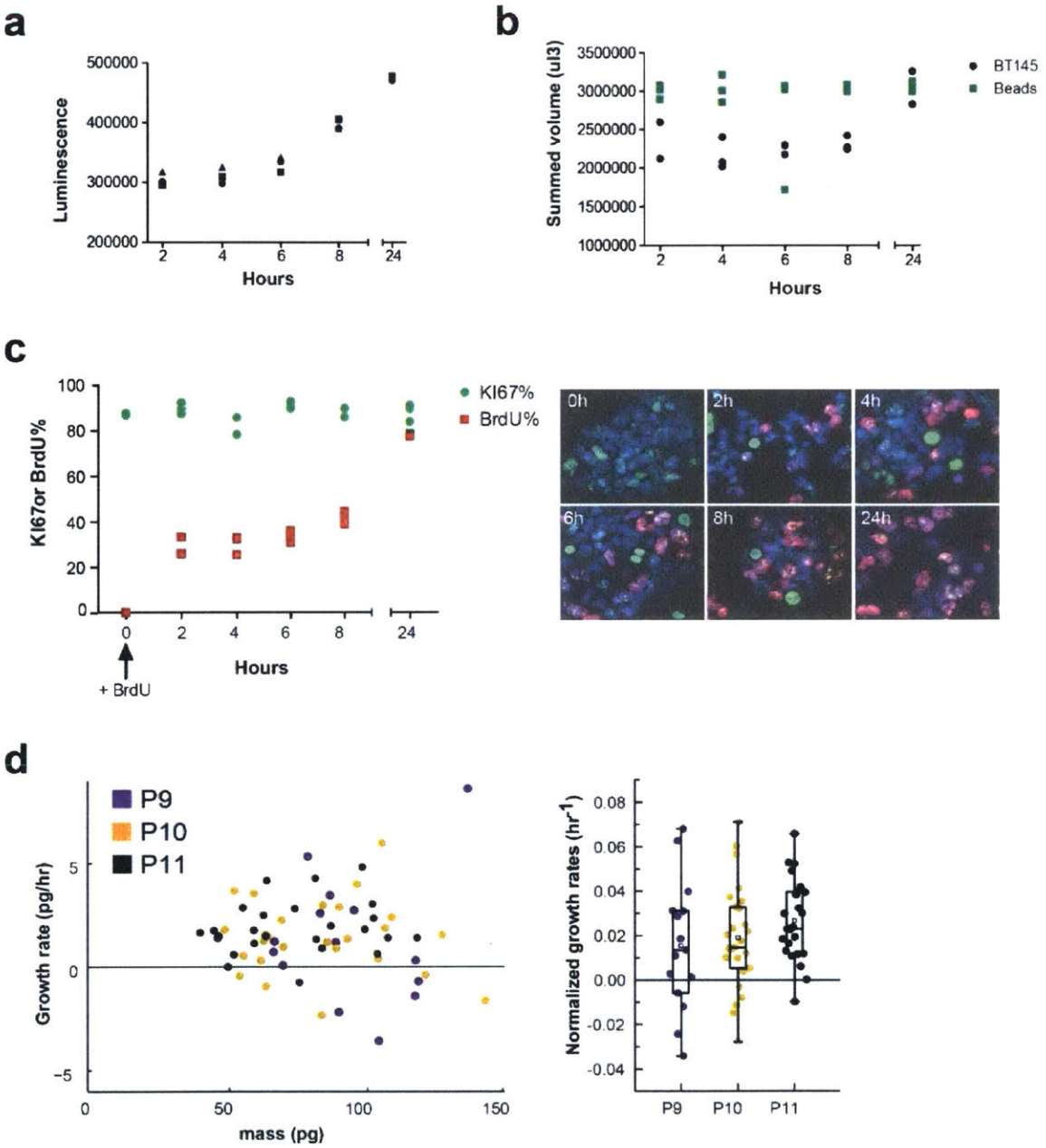

Figure 3-1: Techniques for measuring cell viability and proliferation
(a) Cell titer Glo experiment showing increase in luminescence over a period of 24 hours. (b) Summed volume measurement using Beckmann coulter counter. BT145 cells were dissociated and measured at shown time points and compared to 10 μm beads over a period of 24 hours. (c) Immunostaining of BT145 cells simultaneously for KI67 and BrdU. BrdU was added at the beginning of the experiment after cells were dissociated. (d) Corresponding MAR measurement of BT145. Experiments from (a) and (b) were performed on cells dissociated at P11 and performed in conjunction with the third MAR measurement shown in (d).

3.4 Single-cell tumorsphere formation assay

Note: Parts of this section are adapted from [19]

To determine whether cell proliferation potential could be maintained after passage through the SMR, we isolated single BT145 GBM cells after MAR measurement by modifying our cell-loading protocol to ensure that the bypass channel contained only the cell being measured. The BT145 cell line was chosen because of its high single-cell tumorsphere formation rate of approximately 40%, in addition to reasonably fast growth rates in culture and relative ease of MAR measurement compared to other cell lines.

To ensure that we captured only the cell that was measured, we flushed both bypass channels with fresh media for 1-2 min before starting each cell measurement to clear the channels of all cells. Hence as the cell is subsequently drawn up from the sample vial, there would only be cells in the section of the left bypass channel leading to the sample vial and none in the opposite bypass channel on the right. After measuring a cell, we brought the cell into the right bypass channel and flushed the media in that channel directly into a single well of a low-attachment 96-well plate containing 100μl of media by holding the tubing over the appropriate well of the plate. This procedure was repeated for each cell measured. Because of the time taken for cell extraction and for flushing bypasses before each measurement, total measurement throughput decreased to about 2 cells per hour compared to 3-4 cells per hour without cell isolation.

After completing a measurement, we checked that each well contained a single cell, and assayed the cells over a subsequent period of 2 weeks to observe their ability to form tumorspheres. During this period, we checked the cells every day and took images at the end of the first and second weeks using a bright field microscope. (Images shown in **Figure 3-2** were taken at 2 weeks). Due to the variance in size and cell number in the resulting tumorspheres, we considered any cell that grew and divided into 4 or more cells after the 2 week period to have successfully formed a tumorshpere.

As shown in **Figure 3-2**, 14 (35.9%) of 39 single cells formed tumorspheres compared with 217 (45.2%) of 480 single cells isolated from bulk culture ($p = 0.26$). Hence we concluded that MAR measurement had no statistically significant effect on sphere-formation ability of the cells.

Representative images of a number of neurospheres along with the corresponding mass measurement traces are shown in **Figure 3-2**. As seen from the images of the tumorspheres formed from the isolated single cells, there is substantial heterogeneity not only in the number, size and morphology of cells but also in the organization and compactness of the resulting neurospheres.

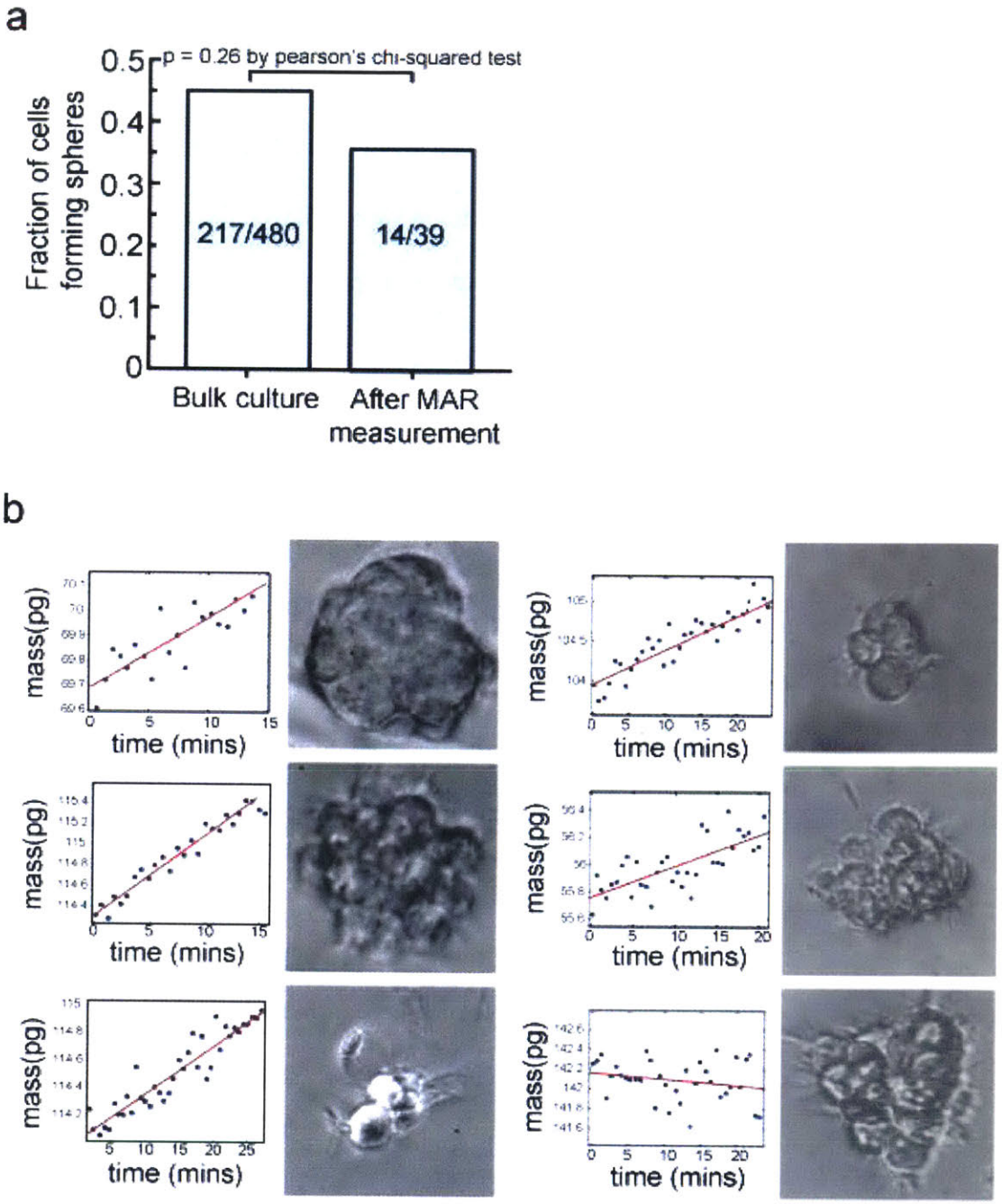

Figure 3-2: Cell isolation in SMR vs bulk culture
(a) The bar plot compares the tumorsphere formation fraction of cells isolated from bulk culture and isolated after MAR measurement. Bulk culture experiments were performed by Cecile Maire
(b) Examples of mass traces of cells and images of the cells after 2 weeks of culture in a 96 well-plate.

Using the same assay, we investigated if cells increasing in mass were more likely to be capable of growth into neurospheres compared to cells losing mass. As shown in **Figure 3-3**, although cells with positive MARs contained a much larger fraction capable of growing into tumorspheres compared to those with negative MARs, the result was not statistically significant ($p > 0.2$ using Fisher's exact test appropriate for very small sample sizes).

The reason for this is a combination of the small number of cells with negative MARs, the low sphere-formation rate in general (only 2 cells grew into spheres among negative MAR cells), and the low throughput of our cell extraction technique. As a result, we were unable to make a definitive statement on the possibility of such a correlation with current techniques. In future work, higher throughput methods of cell-measurement combined with automated extraction, for example by using motorized stages, may provide further insight into this question.

Additionally, even though 2 of the cells capable of sphere formation were measured with a negative MAR, they were losing mass relatively slowly. Hence it is possible that they may have been maintaining a constant mass. It would be important to study such cells in future work where more data is available, to determine if such cells had MARs closer to zero relative to other cells in the same cell line.

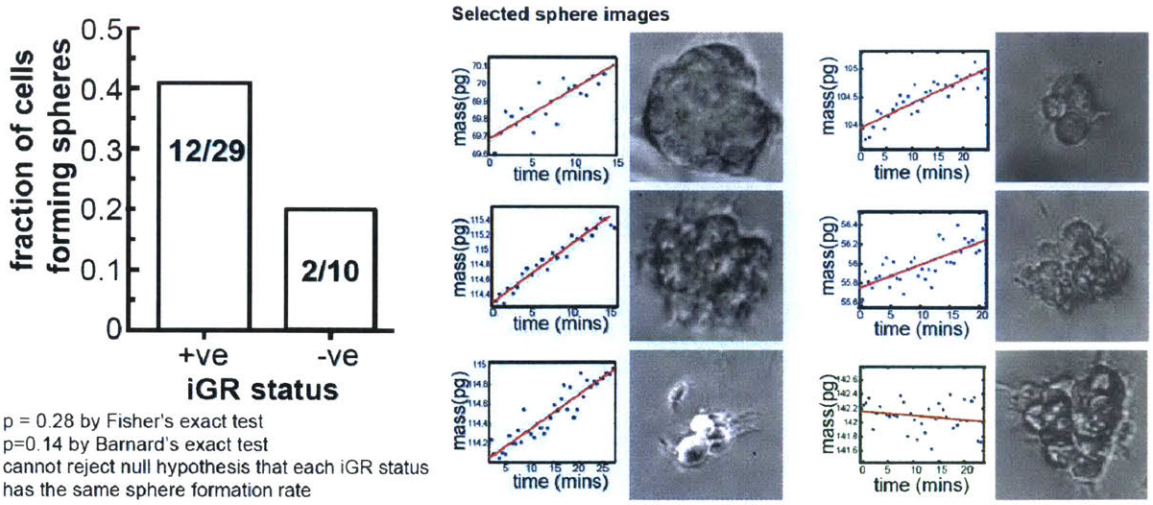

Figure 3-3: Cell isolation: positive vs negative MARs
The bar plot on the left shows the fraction of single cells having positive or negative MARs which are capable of tumorsphere formation. The result is not statistically significant by 2 tests commonly used for small sample sizes. The same example cells from **Figure 3-2** are color coded according to MAR status, positive in purple and negative in green.

3.5 Conclusion

In conclusion, we have shown a variety of techniques that attempt to measure cell proliferation or viability. However, they are all population measurements and have limited ability to obtain meaningful measurements on the time scale of hours. The MAR assay had advantages in both these areas, and may provide a more precise and unique measure of cell proliferation and viability. In addition, we have also demonstrated that the MAR measurement does not significantly reduce the sphere-formation ability of cells, showing that the cells are in good condition for use in downstream assays post-MAR measurement.

Chapter 4

MAR measurement reveals intra- and inter-tumoral heterogeneity, and predicts drug susceptibility and resistance

Note: Most of this chapter is adapted from [19]

One advantage of MAR measurements over the methods outlined in the previous section is its ability to characterize heterogeneity in a culture at the single-cell level. The previous chapter outlined a number of such commonly used measurement techniques to measure cell growth or other markers of proliferation. However, since most require extended culture or cell lysis, the heterogeneity within a PDCL or patient sample cannot be easily measured or monitored continuously and over time.

On the other hand, techniques to investigate the genetic basis for tumor formation, such as deep sequencing or single cell sequencing have become more common. Such approaches aim to elucidate the different subpopulations that form a tumor or that arise after a drug treatment. However, although they provide important genetic and transcriptional characteristics of cells from which predictions can be based, these techniques do not provide direct information on proliferation dynamics and viability.

In this chapter, we use the MAR measurement to explore inter- and intra-tumor heterogeneity in GBM PDCLs. To our knowledge, this is the first attempt at characterizing and comparing heterogeneity, either in tumors or in PDCLs. We envision that the MAR technique, by providing direct information on a physical characteristic of cells relating to their growth and proliferation, will both provide a unique picture of cell heterogeneity as well as complement existing sequencing techniques.

Secondly, we show how the same technique can have utility in a clinical setting as functional measure of drug susceptibility. We hypothesized that cells undergoing apoptosis are likely be losing mass and cells in growth-arrest would likely remain at a constant mass instead of increasing in mass. Hence regardless of mechanism, we expect to observe an average decrease in MAR in a PDCL that is incubated with a drug to which it is susceptible. Even if not all cells are equally susceptible, such as in a heterogeneous tumor, an overall decrease should be detectable if sufficient cells are measured.

In the previous chapter we showed that the MAR measurement is capable of accurately assessing the viability of GBM cultures over a shorter time-frame than traditional measurements such as Cell-titer Glo, and can consistently characterize distributions of mass and MAR in GBM PDCLs. We were able to apply this measurement to PDCLs treated with drugs over different time periods, showing significant changes in MAR profiles of drug-susceptible PDCLs compared to resistant PDCLs. We expect that further refinements of such a technique will allow for more rapid testing of targeted drug therapies, resulting in improved treatment of GBM patients.

4.1 Measurement of 7 GBM PDCLs

4.1.a Significant MAR heterogeneity observed between and within GBM PDCLs and commercial cell line U87

We first attempted to characterize the amount of variation in both mass and MAR within a single PDCL, between PDCLs, and between successive culture passages of a single PDCL. In total, we measured MARs of single cells from 7 different GBM-PDCLs with diverse genotypes (Table 1) over at least three successive passages.

We also compared the MAR vs mass profiles of these PDCLs to two lymphoid cell lines (Mouse lymphoblast cell line L1210 and lymphoblastoid cell line BAF3-BCR-ABL) that are known to increase in mass exponentially in a very homogeneous way in the SMR [6].

The commercial cell line U87, a commonly used glioblastoma cell line available from ATCC, was measured using the same protocol for comparison to the PDCLs.

Pooled data from three measurements are shown as MAR vs mass in **Figure 4-1**. All cell lines are plotted along identical axes to allow for a clear comparison of the diversity in both MAR and mass within and across cell lines. Lymphoid cell lines are shown in gray and various GBM PDCLs and cell-lines are shown in color.

MAR measurements revealed significant inter- and intra-PDCL heterogeneity across the seven PDCLs with single-cell diversity in both MAR and mass. These findings were in stark contrast with the homogeneity of MARs observed in the conventional hematopoietic cell lines, such as the L1210 and the BAF3 cell line (first 2 plots of **Figure 4-1**). Such homogeneity did not appear to be related to the advanced age and high passage-number of these lines, since the conventional GBM cell line U87 also exhibited significant MAR heterogeneity, a pattern common to many of the PDCLs and characterized by a large spread of growth rates with many cells having negative or near-zero growth rates.

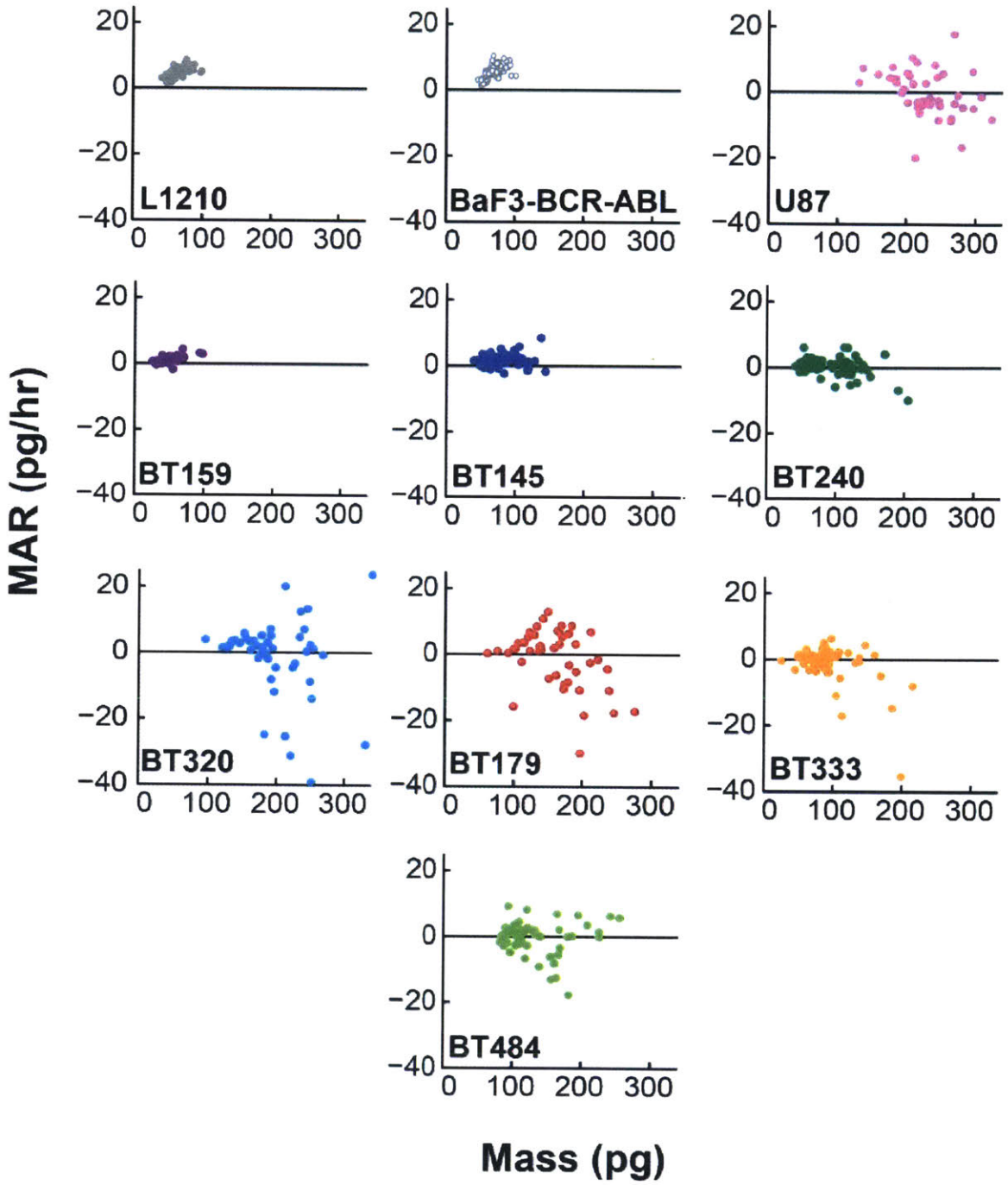

Figure 4-1: MAR vs mass profiles for all cell lines
MAR vs mass profiles for 2 murine lymphoid cell lines, GBM cell line U87 and 7 GBM PDCLs shown on identical axes for comparison.

Among the GBM-PDCLs, some lines like BT159 and BT145 display more homogenous patterns of mass accumulation. In particular, BT159 resembled the lymphoid cell lines, with all positive MARs that monotonically increased with cell mass. The only apparent difference was that BT159 had a slightly lower MARs and a small percentage of cells with negative MARs. The relatively homogeneous MAR profile of this cell line, together with it having a large proportion of cells with positive MARs, is consistent with immunohistochemistry analysis showing that a majority (80%) of the cells were positive for the proliferation marker KI67.

At the other extreme, BT320 and BT179 have the most heterogeneous phenotype, which appears to be consistent over consecutive passages (**Figure 4-3**). Immunohistochemistry analysis (**Figure 4-2**) is consistent with our MAR data, showing that BT320 and BT179 have high levels of heterogeneity. Interestingly, we noticed that the larger cells (mass above 150 pg) are not always dying and losing mass. Some have positive MARs which may be related to the giant-cell histopathological features sometimes observed in GBM.

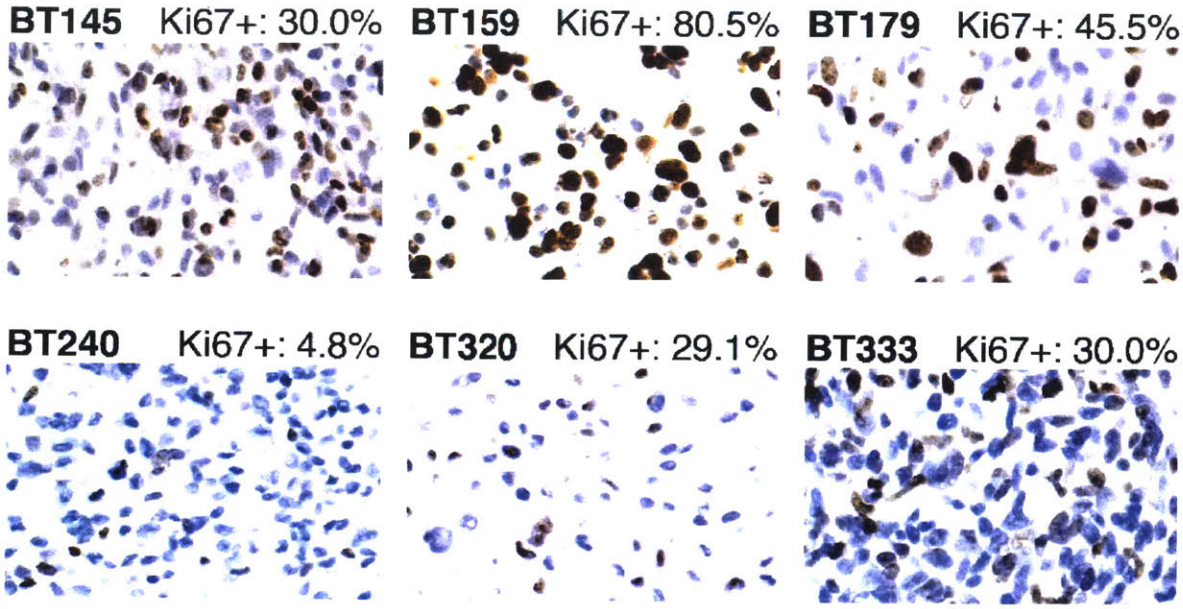

Figure 4-2: Staining and percentage of cells positive for KI67
Representative staining results from immunohistochemistry for KI67 on BT145, BT159, BT179, BT240, BT320, and BT333 cell lines. Results are quantified as percentage of total cells stained positive. Staining performed by Cecile Maire.

In all the cell lines measured, MAR measurements enabled the delineation of different growth populations, identifying cells of both large and small masses having positive, near-zero and negative MARs. GBM tumors have been shown to contain a diverse mixture of growing, quiescent, senescent and dying cells [20, 21]. Thus, the heterogeneity of MAR and mass observed in these PDCLs seem to parallel the known morphological diversity and heterogeneity in growth characteristics of cells from primary GBMs.

4.1.b Maintenance of MAR heterogeneity across culture passages

In **Figure 4-3**, normalized MARs, or MAR per unit mass of the same data from **Figure 4-1** are shown to better illustrate the maintenance of heterogeneity in each PDCL across successive culture passages in bulk culture. Each of the 3 measurements for every PDCL is plotted separately, showing that the extent of heterogeneity in individual PDCLs as well as in the U87 cell line was maintained across consecutive passages. This result suggests that intra-tumoral diversity in growth is an inherent property of GBM PDCLs even during in vitro propagation.

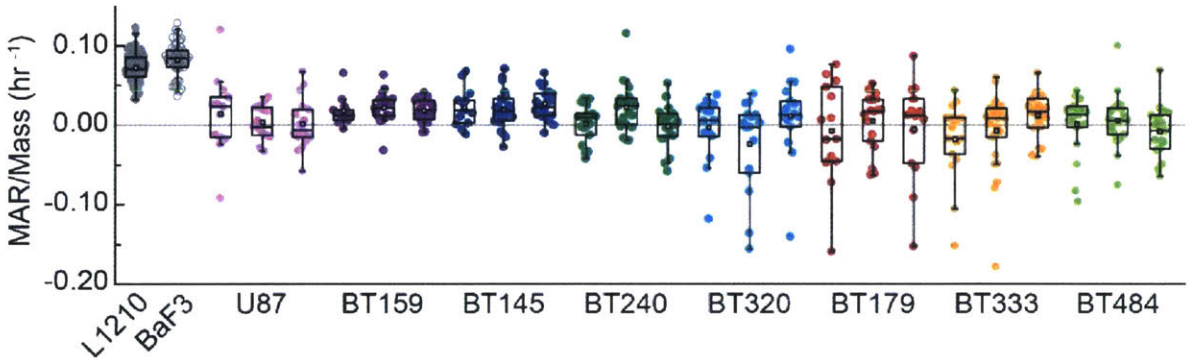

Figure 4-3: MAR per unit mass for all cell lines separated by passage
MAR over mass or normalized MAR for all cell lines showing measurements over successive passages. For L1210 and BaF3-BCR-ABL which show very little variability across measurements, pooled data from multiple (5-6) measurements are plotted together. For all U87 and GBM PDCLs, paired t-tests between measurements all have $p>0.05$.

4.2 Drug susceptibility measurements

4.2.a Desirable characteristics of a drug susceptibility assay

An ideal functional assay for predicting therapeutic response in patients with cancer would (1) accurately measure responses to both single drugs and combinations of drugs; (2) require minimal sample input; (3) avoid artifacts that result from long-term in vitro culture; (4) resolve therapeutic response at the single-cell level; (5) obtain results in a sufficiently short time frame to allow for therapeutic decision making; and (6) maintain cell viability to allow for further functional and molecular assays downstream of the measurement. To our knowledge, no current technique meets all of the above criteria. Such an assay would be useful for predicting therapeutic susceptibility in a variety of contexts, not only in assessing highly heterogeneous primary tumor samples, but also in assessing residual disease following therapy or in isolated circulating tumor cells.

The MAR assay fulfils most the above requirements, providing an approach for functionally assessing the therapeutic sensitivity of single cancer cells. In particular, we show a rapid detection of drug response on the order of 1-2 days (points 3 and 5), and have demonstrated the maintenance of cell viability (point 6) that is essential for compatibility with downstream functional, molecular and genetic assays. The ability of the MAR technique to maintain viability of the cells after measurement has been validated using the single-cell neurosphere formation assay described in detail in Chapter 2.

However, to fully achieve quantification at a single cell level (point 4) and to test combinations of drugs (point 1), higher throughput techniques to measure MAR will be required to obtain sufficient numbers of cells in a reasonable time frame.

Here we demonstrate the ability of the MAR assay to functionally assess the therapeutic sensitivity of single cancer cells, either in the presence or absence of cancer therapeutics. After incubation of tumor cells with drug, the MAR assay was able to detect statistically significant changes in the profiles of susceptible GBM PDCLs over a period of 24-48 hrs, predicting therapeutic response without the need for extended culture.

4.2.b Predictions of drug susceptibility based on Genetic background of GBM PDCLs

Although GBM is highly resistant to most therapeutics, the Ligon lab has recently shown that some GBM-PDCLs are sensitive to targeted MDM2 inhibition [22]. MDM2 is part of the P53 signaling pathway, which is altered in 87% of GBM tumors. MDM2 is amplified in 14% of tumors tested [13] and tumors containing this mutation would be especially susceptible to MDM2 inhibition.

In bulk tumors and cultures, MDM2 inhibitors are known to induce responses in cells in which wild-type TP53 is expressed and MDM2 expression is amplified, whereas cells with mutant or deleted TP53 are completely resistant to MDM2 inhibitors.

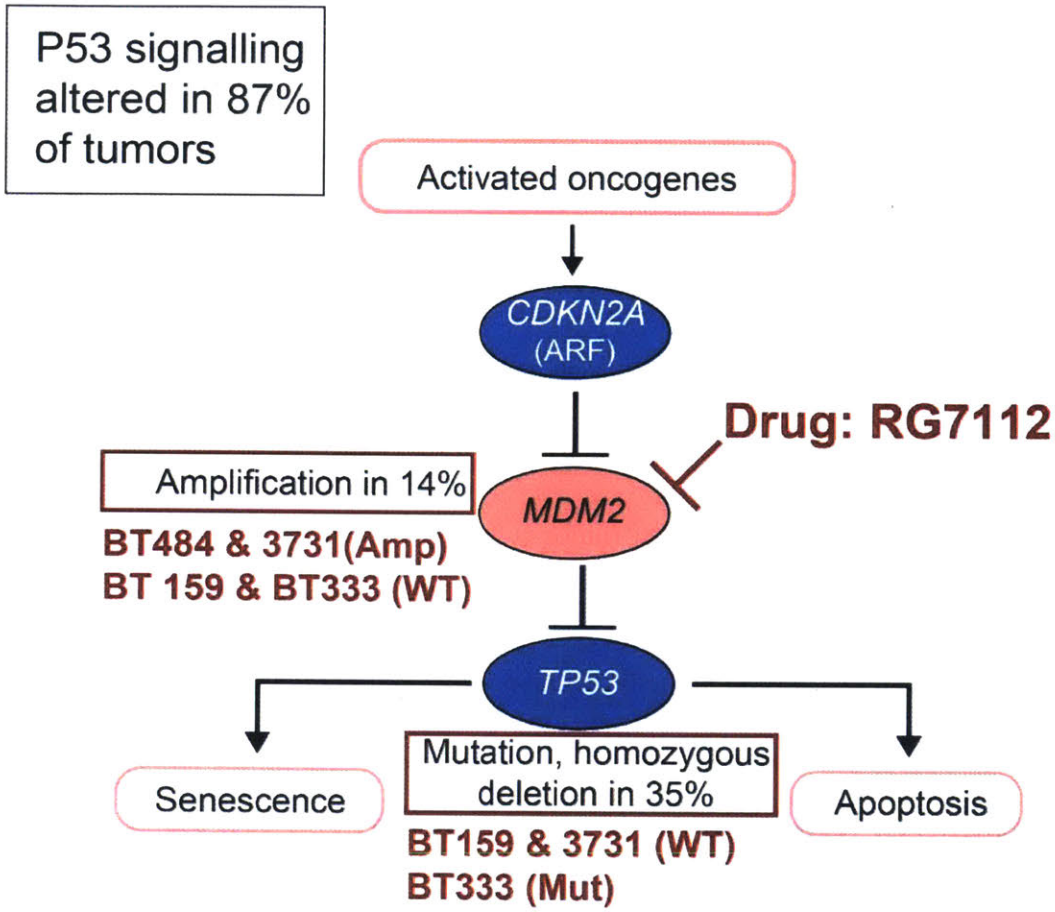

Figure 4-4: P53 Signaling pathway and relevant PDCL mutations
Signaling pathway involving *P53* and *MDM2*. The experimental drug RG7112 inhibits *MDM2*. The *MDM2* and *TP53* status of all tested cell lines are highlighted in red. According to the pathway, we expect that cell lines with wild-type *TP53* and amplified *MDM2* expression would be most susceptible to the drug. The original pathway diagram is from TCGA 'Comprehensive genomic characterization defines human glioblastoma genes and core pathways' *Nature* 2008

In the first case, it is theorized that cells with amplified MDM2 expression are relying on the increased activity of MDM2 to suppress TP53 and hence avoid apoptosis. This would make them highly sensitive to any intervention that reduces MDM2 activity levels.

In the second case, cells with mutant or deleted TP53 are resistant to the MDM2 inhibitor because TP53 is downstream of MDM2. The existing mutations or deletions that inactivate or lower the activity of TP53 already allow a cell to escape apoptosis, hence adding an inhibitor to suppress MDM2 activity would not have any additional effect.

A third case involves tumors that express wild-type TP53 but also have wild-type MDM2. Cells from such tumors have been shown to have unpredictable sensitivity to MDM2 inhibitors both in GBM and other tumor cell types [23]. This is hypothesized to be because we cannot be sure if the cells are relying primarily on this pathway for survival, hence we cannot predict how effective a drug inhibiting this pathway will be.

4.2.c Results of drug treatments on five GBM-PDCLs

We used the MDM2 inhibitor RG7112, a compound that is being evaluated in clinical trials [24], to determine how single-cell MAR responses of five GBM-PDCLs across this spectrum of MDM2 and TP53 mutant backgrounds might empirically correspond with genetics and Cell Titer Glo bulk sensitivity measurements. The results are shown in **Figure 4-5**.

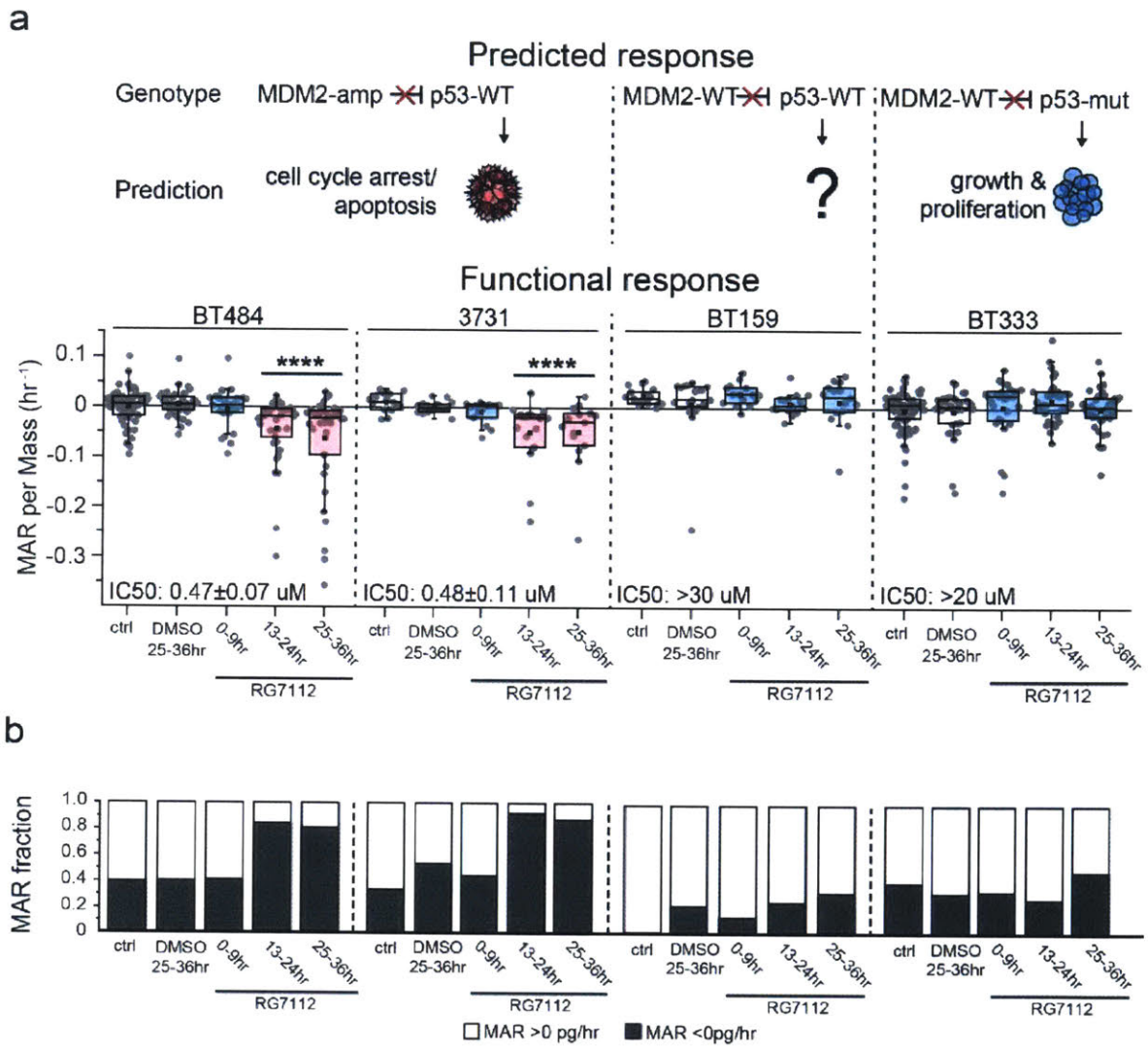

Figure 4-5: Results of MAR drug-susceptibility experiments
Incubation with MDM2 inhibitor RG7112 results in highly significant MAR changes in susceptible cell lines but not in resistant cell lines. Tests with BT159 in which prediction would be unclear based on genetic analysis show the unique ability of MAR measurement to asses drug susceptibility. (a) MAR per unit mass for each cell line over 36 hrs of culture with drug compared to DMSO control. ****$p < 0.0001$ for the highlighted segments. From left to right, n = 59, 37, 25, 38, 37; 16, 18, 15, 15, 15; 15, 16, 14, 16, 15: 69, 32, 27, 37 and 38 cells. (b) Bar plots showing fraction of cells that have positive (shaded) and negative (unshaded) MARs, showing that susceptible cell lines have much larger fractions of cells with negative MAR at the 13-24 hr and 25-36 hr time points.

BT484 and 3731 cells, in which wild-type TP53 is expressed and MDM2 expression is amplified, had mostly negative MARs after incubation with 1 μM RG7112 for 13–24 h and had normalized MARs that were statistically significantly lower than that of the control experiments in DMSO ($p<0.0001$ in all cases listed in figure). With increasing drug incubation times, the number of cells with negative MARs further increased for the 25–36 h time-point, in which more than 80% of cells were losing mass in both PDCLs. For BT484, we conducted a single measurement of the 41-48 hr time point (not shown in figure), in which greater than 95% of the cells had negative MARs.

In comparison, BT333 cells, which express wild-type MDM2 and mutant TP53 and are not expected to be susceptible to RG7112, showed no significant change in MAR at all time points up to 36 hr compared with a DMSO-treated control. In addition, the fraction of cells with negative MARs did not increase significantly.

As shown in **Figure 4-6**, the susceptible cell lines BT484 and 3731 showed some decrease in cell mass along with MAR, although the effect is large for 3731 and very minor in BT484. On the other hand, there was no obvious change in mass profiles of cells in BT333 and BT159.

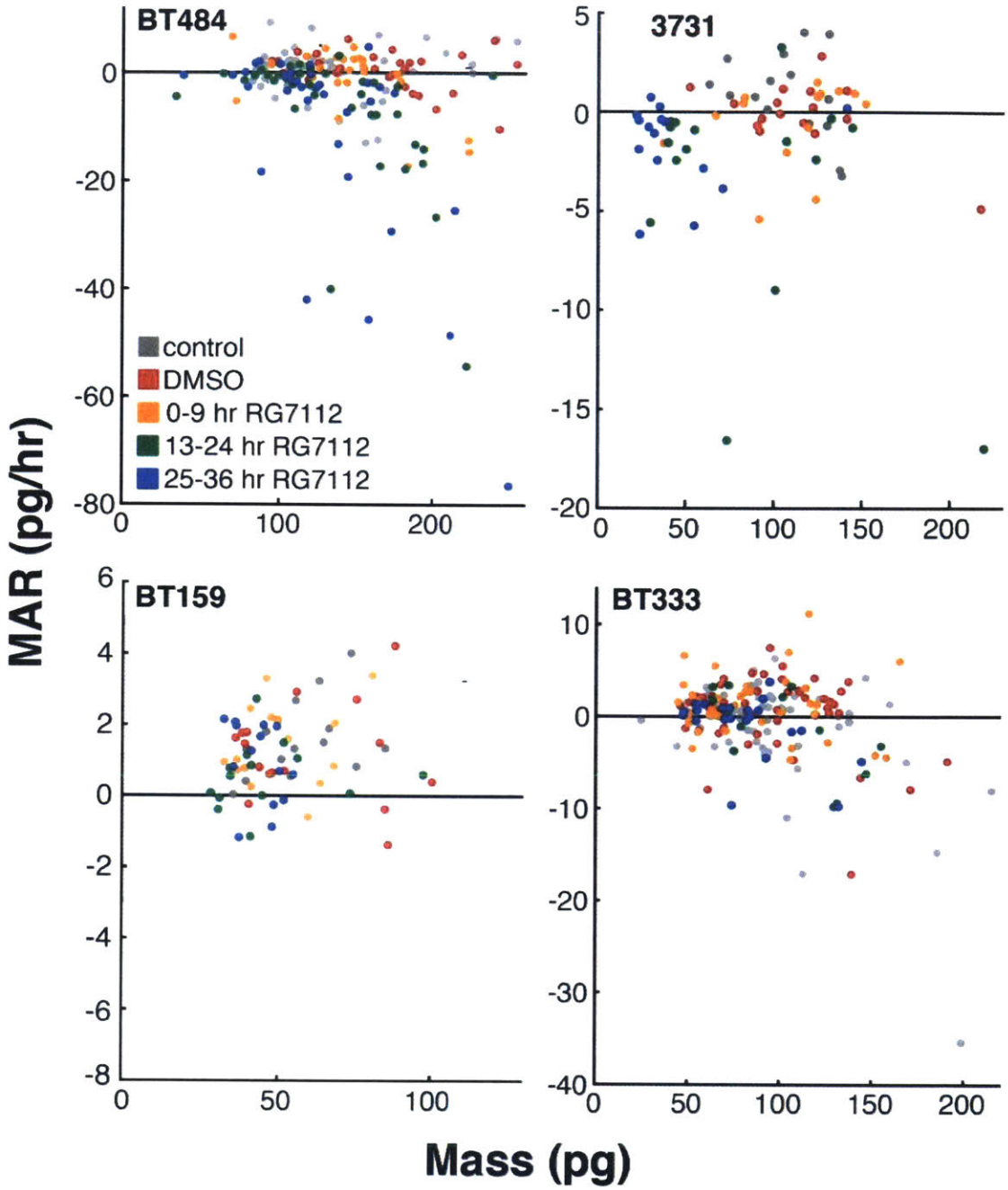

Figure 4-6: MAR vs mass in response to drug.
Plot of MAR vs mass for BT484 and BT333 showing that cells decrease in mass as well as MAR at increased incubation times with RG7112, although the effect is small in BT484 and very large in 3731. BT159 and BT333, which are not affected by the drug and do not display a general decrease in mass, are shown for comparison.

In contrast to the predicted sensitivity and resistance of the above 3 lines, the response of cells from the BT159 line, which express wild-type MDM2 and TP53, was not clearly correlated with the MDM2 and TP53 genotype. For example, targeted and whole-exome sequencing of BT159 cells, which express wild-type MDM2 and TP53, showed no mutations or copy number alterations in TP53, TP63, TP73, CDKN2A, MDM4, mitochondrial apoptosis mediators, or other p53-related genes that could mediate MDM2 inhibitor resistance (see Table 1).

However, BT159 showed no evidence of single-cell response by 36 hr using MAR measurements, similar to the complete resistance exhibited by TP53-mutant BT333 cells (**Figure 4-5**). It also showed no dramatic increase in cells with negative MARs, as shown in **Figure 4-5**(b). This example highlights how the MAR can be used to assess drug susceptibility even in cases where predictions from genetic markers are unclear.

4.2.d Validation with Cell Titer Glo viability measurements

MAR measurements for all lines were consistent with the response in viability as measured by Cell Titer Glo after 72 h of RG7112 exposure (**Figure 4-7**). Both cell lines that showed decreases in MAR had IC50s of lower than 0.5 μM, while cell lines that did not show decreases in MAR had IC50s greater than 20 μM, indicating that they were not susceptible to the drug at a typical physiological dose.

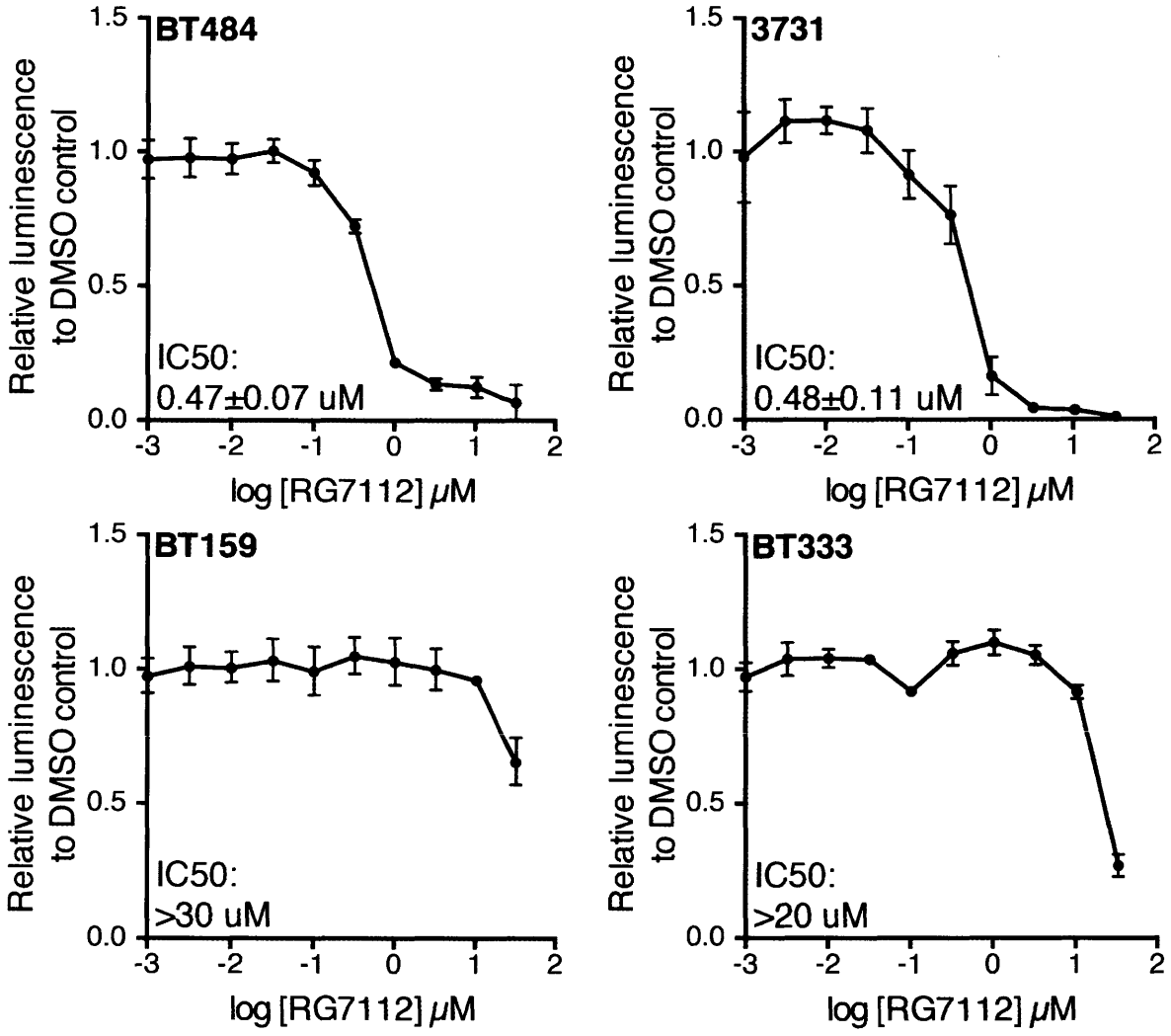

Figure 4-7: IC50s for cell lines using Cell titer glo
Cell-titer glo experiments (72 hr incubation) to determine IC50s for the respective cell lines measured. Both BT484 and 3731 have relatively low IC50s. BT 159 and BT333 both have IC50s greater than 20 μM.

4.3 Discussion

4.3.a Applicability of MAR measurement to downstream assays

An important advantage of MAR measurements is that cells remain viable throughout the measurement and are available for further analysis. We have shown one example of extraction of cells post-MAR measurement for analysis by performing single-cell tumorsphere formation assays as described in Chapter 3. If the volume of media used to flush the cell out of the chip can be reduced significantly, for example by refining the cell extraction technique using smaller or shorter tubing, one can perform analysis on other non-functional biomarkers (e.g., genetics, gene expression and chromatin modifications) at a single cell level. This ability will ultimately allow for correlations between single-cell changes in MAR and a variety of functional outcomes, gene-expression, and genetic and epigenetic characteristics.

Further studies will be needed to assess the effects of passage through the SMR on aspects of tumor cell biology, including changes in the transcriptome, genome or proteome. Previous studies have found that cellular and genomic properties of single cells can be measured using techniques such as RNA sequencing and are well-preserved following exposure to microfluidic environments [25]. Hence single cell sequencing may provide further insights when combined with the MAR measurement.

4.3.b Comparison to other functional assays

A number of recent studies have used various functional approaches to predict therapeutic sensitivity of individual cancers. For example, one group used standard proliferation-based assays to quantify therapeutic susceptibilities of bulk cultures of PDCLs [7]. The results from this ex vivo screening predicted the response of in vivo xenografts to combination therapies. However, this population-based approach is unable to capture heterogeneity in response at a single cell level, and its usefulness for clinical decision-making is constrained by the time required for creation of the PDCLs and for performing the necessary assays.

Another recent study presented a functional approach called 'dynamic BH3 profiling', in which therapeutic interventions are applied to cell lines or clinical tumor isolates, and the percentage of cells that undergo mitochondrial outer membrane permeabilization is measured after introduction of a pro-apoptotic BH3 peptide [4]. This technique was able to predict which patients would respond to a given therapy across multiple cancer types. However, this approach requires the cells to be permeabilized, which makes implementation of downstream assays more difficult, and cannot distinguish between subsets of cells in a heterogeneous sample.

MAR measurement addresses most of these limitations by assessing therapeutic susceptibility in single live cells, but is has its own set of constraints. Most importantly,

PDCL generation is still required, and a significant period of in vitro culture of a minimum of 24 hours is still necessary before a response to applied therapeutics can be observed, at least in the case of GBM cells. Hence the MAR measurement can reduce, but does not completely eliminate, the time required in in-vitro culture. In addition, the MAR assay currently requires cells to be in a single-cell suspension or clumps of cells small enough to fit into the resonator channel, which may limit the types of cancers that the MAR measurement can be applied to.

4.3.c Limitations of MAR measurement as a drug susceptibility assay

The most significant shortcoming of the MAR approach in assessing drug susceptibility is a potential bias toward only measuring cell-intrinsic drug susceptibility. Microenvironmental interactions within the tumor have the potential to influence in vivo drug responses, and cells may lose 'memory' of such interactions if they are removed from the tumor and cultured for extended periods [26].

There have been recent advancements in using implantable devices to test drug effects directly in the tumor environment, but such approaches are only compatible with solid tumors, require tumors that are sufficiently large and easily accessible, and require an additional biopsy for removal of the device [27].

Although this problem is common to most functional assays, there may be ways to address the role of microenvironmental interactions. One possibility is to culture tumor cells together with stromal cells or immune cells in the presence of drug before measurement.

Alternatively, one can use the MAR measurement to monitor patient response by performing the measurements directly on cells extracted from patient biopsies. For example, patient tumor cells could be analyzed with MAR measurements immediately before treatment and at selected time points after treatment. However, further development of cell-handling and processing, and increased throughput of the MAR measurement will be required in such a case.

4.4 Conclusion

In conclusion, we have demonstrated the potential of MAR as a tool for understanding and characterizing heterogeneity in GBM PDCLs, and its utility for functional drug susceptibility testing by successfully detecting the effects of a drug after an incubation period of 24-36 hrs. We validated the drug-susceptibility results with Cell-titer glo measurements of IC50 values for each cell line.

Future work with larger patient samples and increases in measurement throughput have the potential to provide correlations between MAR profiles and patient outcome, which

will be useful both in understanding the disease and in devising new treatment regimes. The availability of cells post-measurement also provides the potential for further insights into correlation between MAR values and other functional and genetic characteristics at a single cell level. However, more work needs to be done to increase throughput of the assay and to account for microenvironmental effects on drug response.

4.5 Appendix: GBM PDCL genetic analysis

PDCL	Diagnosis	EGFR	CDK4	CDK6	PTEN
BT145	GBM Astrocytoma IV	WT	WT	WT	WT
BT159	GBM Astrocytoma IV	WT	WT	WT	WT
BT179	GBM Astrocytoma IV	AMP	WT	WT	L70_splice
BT239	GBM Astrocytoma IV	Mut p.R521K	WT	WT	WT
BT240	GBM Astrocytoma IV	WT	WT	WT	WT
BT320	GBM Astrocytoma IV	WT	WT	WT	MUT p.G132A
BT333	GBM Astrocytoma IV	AMP, MUT p.F254I	WT	WT	WT
BT484	GBM Astrocytoma IV				MUT p.C136Y
3731	GBM Astrocytoma IV				

PDCL	PDGFRA	MET	CDKN2A	NF1	MDM2	RB1	TP53
BT145	WT	WT	HOMDEL	WT	WT	WT	WT
BT159	WT	WT	HOMDEL	MUT p.D176E	WT	WT	WT
BT179	WT	WT	HOMDEL	WT	WT	WT	MUT p.I255T
BT239	WT	WT	HOMDEL	MUT L249fs	WT	WT	WT
BT240	WT	WT	HOMDEL	WT	WT	WT	MUT p.S227Y
BT320	WT	WT	HOMDEL	WT	WT	WT	HOMDEL
BT333	WT	WT	HOMDEL	MUT p.D176E	WT	WT	MUT p.V173M
BT484					AMP		WT
3731					AMP		WT

Table 1: Muation analysis of GBM PDCLs. Abbreviations: AMP, amplification; MUT, mutation; HOMDEL, homozygous deletion. Data from Cecile Maire.

Chapter 5

Estimation of position-dependent mass changes by combining multiple resonant mode frequency data with image data

5.1 Introduction

Measurements of suspended cell buoyant mass in the SMR require complete passage of a cell through the cantilever, with the measured variable being the maximal frequency deviation from the resonant frequency of a cantilever containing only culture media (**Figure 5-1**). This measurement technique assumes passage of the cell across defined locations on the cantilever, such as a position close to the tip of the cantilever when the 1st resonant mode is measured, and the antinode position of the 2nd resonant mode when

the 2nd resonant mode is measured. Since the measurement is consistently taken at the same positions, a simple linear conversion factor can be used to convert the frequency change to a value for buoyant mass as long as the frequency change is small relative to the resonant frequency [3]. Hence position information of the cell is not required and optical access to the interior of the cantilever has been unnecessary for the previously described applications.

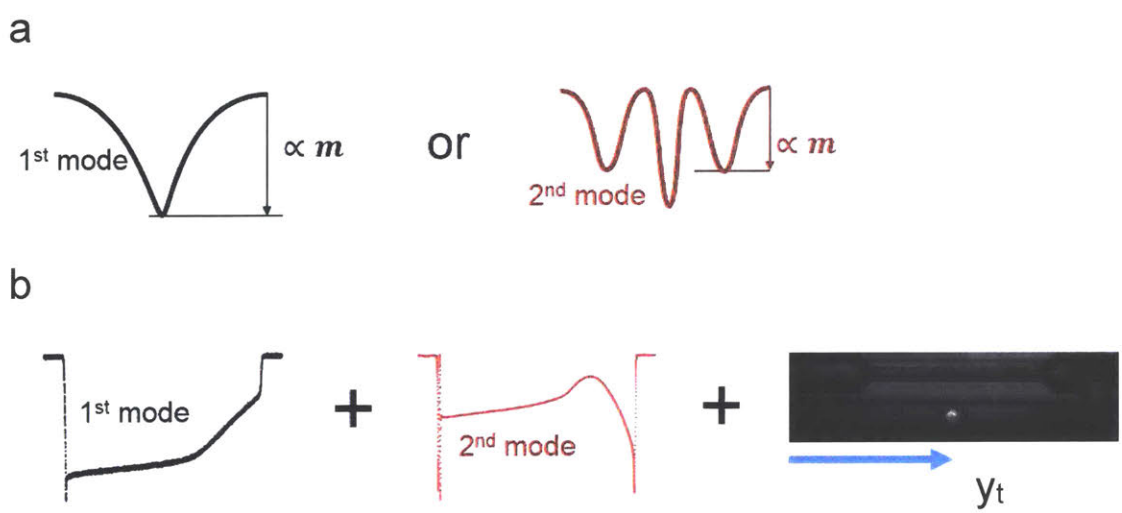

Figure 5-1: General schematic for multimode mass estimation with imaging
Schematic showing (a) previously described technique for estimating mass of a single particle passing through the cantilever. Note that only one mass measurement is made for the entire particle transit, using the peak height of the main or side peak. (b) Proposed technique for estimating mass of the particle at particular points in its passage through the cantilever, by combining frequency data from one or more modes with image data showing the position and extent of the cell.

Here we develop a system incorporating an infrared camera to gain optical access to the channel within the cantilever. We also develop processing techniques to synchronize image data acquisition to resonant frequency measurements. We aimed to measure position-dependent mass changes in a cell.

Incorporating position information could allow the mass change of the cell as it passes through the cantilever to be estimated, if the change is large enough relative to the measurement uncertainty of the technique. We aimed to use such a technique to measure changes in water content of a cell as it deforms through a constriction within the cantilever, which is expected to occur to some extent since aquaporins on the cell membrane allow free movement of water through the membrane

The change in density and water content of a cell is currently unknown, and there is to our knowledge no attempts in the literature to measure such a change. Most analysis and models of cell deformation in microchannel constrictions and micropipette aspiration assume that mass and volume are conserved [28, 29]. Entry or exit of water from a cell under mechanical pressure could lead to changes in the density and material properties of the cell, with important implications for such cell deformability measurements.

5.2 Theory

Since we have access to image data from the infrared camera, we are able to estimate both the position and extent of the cell, allowing for a first-order estimation representing the cell as a uniform mass distribution from normalized position $z-l/2$ to $z+l/2$ along the length of the cantilever.

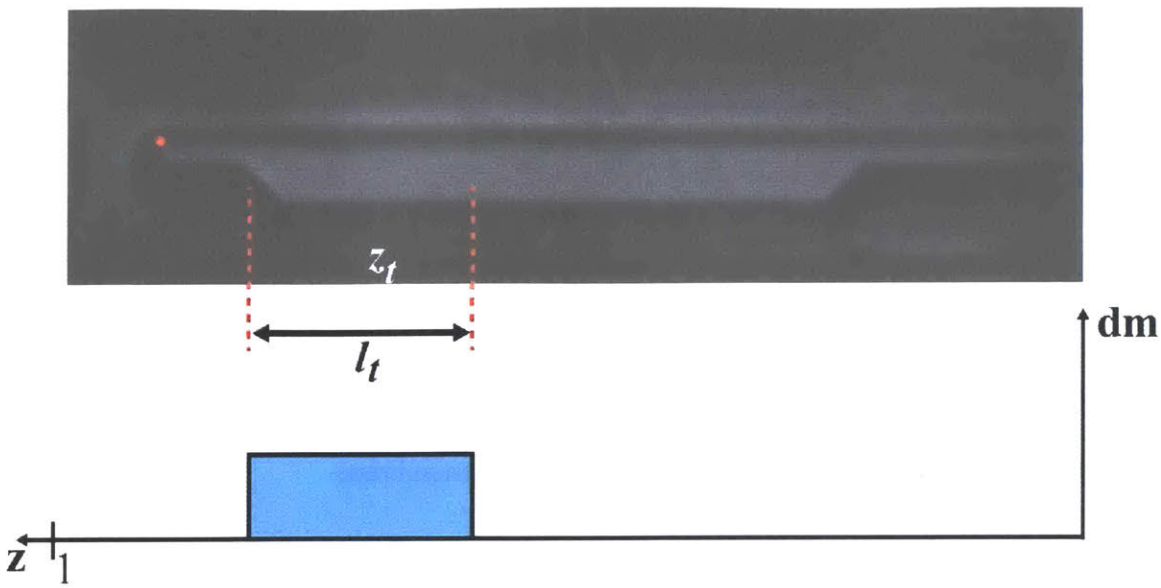

Figure 5-2: Simple model of cell dimensions
Simple schematic showing how the dimensions of a cell are extracted from an image. The two ends of the cell (red dotted lines) are identified, and the position of the cell is taken as the mid-point between these points. The length of the cell is the distance between the 2 points. The cell is represented as a uniform mass distribution (blue box) with a fixed mass/unit length to be estimated. The red dot shown in the image is the point in the image used as an anchor point from which all other measurements are taken. It is helpful in case there is camera movement between experiments.

To relate frequencies in multiple resonant modes to position data, we use the approach first suggested by Dohn et. al. [30] and used by Cermak and Olcum et. al. [31] to estimate particle trajectories using frequency data from 4 resonant modes.

The relative frequency shift $\frac{\omega_{\Delta m,n}}{\omega_n}$ of a resonant cantilever can be related to the total mass of the resonating system m_0 (including both cantilever and fluid), its resonant mode n, and a loaded point mass of Δm and position z using the following equation:

$$\frac{\omega_{\Delta m,n}}{\omega_n} = \frac{s_n}{\sqrt{1 + \frac{\Delta m}{m_0} U_n^2(z)}}$$

Or according to our boxcar uniform mass distribution model:

$$\frac{\omega_{\Delta m,n}}{\omega_n} = \frac{s_n}{\sqrt{1 + \frac{1}{m_0} \int_{z-l/2}^{z+l/2} dm\, U_n^2(z)}}$$

Where s_n is a sensitivity adjustment parameter to account for varying sensitivity in the second and higher modes. s_n is normalized to the first mode.

The relative effect of the loaded mass is modulated by the normalized time-independent mode shape equation *U(z)* shown below:

$$U(z) = \cos(k_n z) - \cosh(k_n z) + \mathrm{c}_n(\sin(k_n z) - \sinh(k_n z))$$

Where $k_n$is the nth root of $\cos(x) - \cosh(x) = -1$ and $\mathrm{c}_n = \frac{sin(k_n) - sinh(k_n)}{\cos(k_n) - \cosh(k_n)}$.

z is normalized to the length of the cantilever. This equation gives a maximal value at the antinodes and 0 at the nodes of each mode, and is normalized so that the integral of *U(z)* over *z* is 1.

We then attempt to minimize the residual squared error given below in order to estimate the fractional change in mass $\frac{dm}{m_0}$:

$$\chi^2\left(z, \frac{dm}{m_0}, s\right) = \sum^{F}\sum_{n=1}^{N} \frac{1}{\sigma_n^2}\left(\frac{\omega_{\Delta m,n}}{\omega_n} - \frac{s_n}{\sqrt{1 + \int_{z-l/2}^{z+l/2} \frac{dm}{m_0} U_n^2(z)}}\right)$$

Where F denotes the desired image frames to be optimized against. σ_n^2 is optional and represents the standard deviation of respective modes. It can be used to normalize the weights of each mode if necessary.

5.3 Coarse alignment of image and frequency data

The first and second resonant mode frequency signals measured as a cell passes through the cantilever need to be matched to the corresponding image data obtained from the infrared camera. In addition, due to the large file size of the image data, it is desirable to save only image data in which the cell is within the cantilever and omit image data at all other times when there is no cell in the cantilever. If we exclude such extraneous image data, we can reduce the file-size of the saved image data by at least 90% in a typical experiment where cell concentrations are approximately 500,000 per ml.

Our solution to both these problems is to use the frequency data to control saving of the image files from the camera. A user-defined threshold for change in the derivative of the frequency signal in first mode is used as a trigger to start saving images. The frequency at this point is recorded, and image saving is stopped when the frequency measured rises above the recorded frequency plus some offset. Both the start and end times of the peak and the series of image files from the cell are labeled with the same identifying number, so that the image and frequency signals for each individual cell can be subsequently matched and aligned.

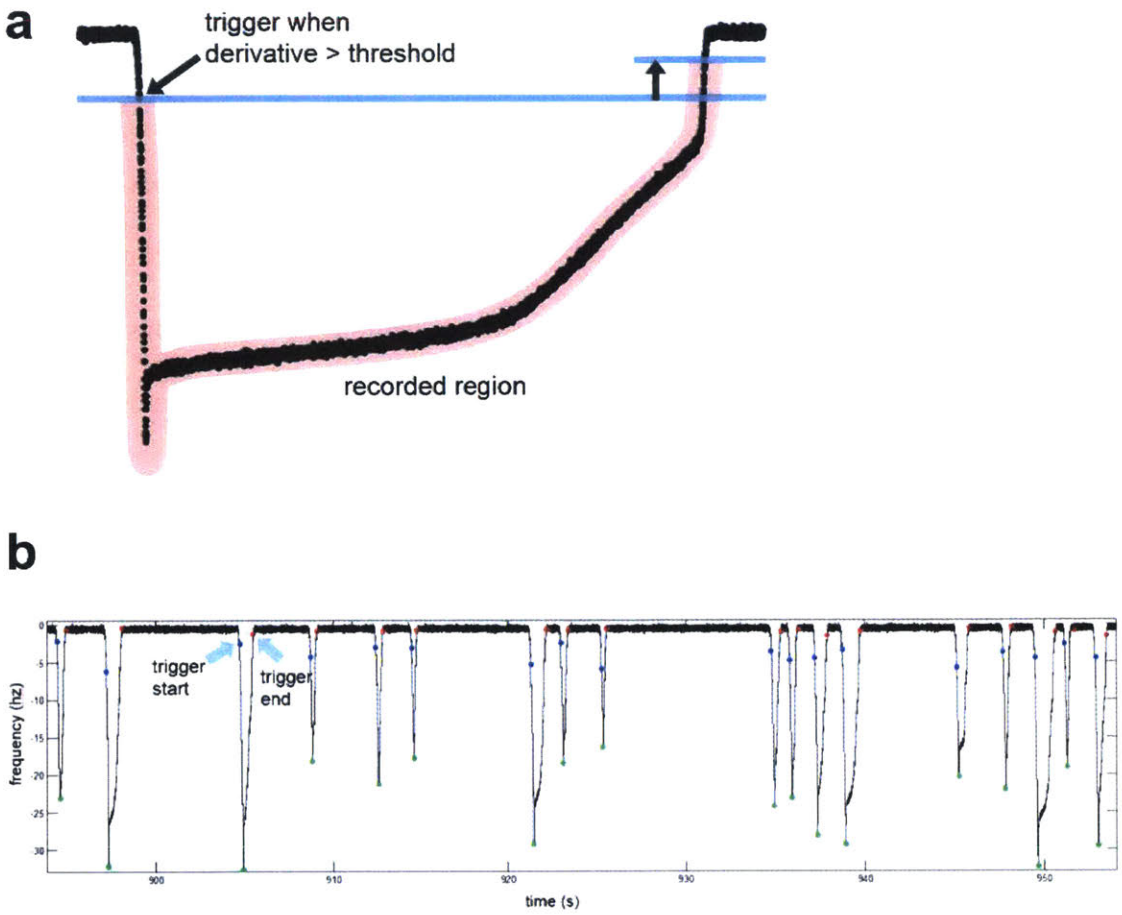

Figure 5-3: Triggering using first mode peaks
(a) Schematic showing the section of a first mode peak during which image data is saved (highlighted in red) and given an identifying number for subsequent matching to the corresponding peak. The start of image recording occurs when the magnitude of the derivative of the signal exceeds a given threshold. The frequency value at this point is recorded (horizontal blue line) and image recording is stopped when frequency next reaches a fixed offset above that value (shorter blue line). (b) A representative stretch of raw first-mode frequency data with blue dots denoting the start of image saving and red dots denoting the end of a recording

5.4 Obtaining normalized position information from image frames

When the camera is set up, we ensure that the long edge of the cantilever in the image is exactly parallel to the y-axis of the camera's detector, so that lengths along this axis can be determined simply by counting numbers of pixels in the y-direction. The length of the cantilever from base to tip is measured in pixels (1140 pixels in our setup and magnification) and all other measured lengths and cell positions were normalized to this value.

All cell positions are measured relative to a well-defined reference or anchor point at the end of the inner channel wall of the cantilever (shown in **Figure 5-2**), for which the length in pixels from the base of the cantilever is known. This reference point allows us to adjust for movement of the camera during and between experiments.

The position and length of the cell is estimated by manually selecting the y-axis values of the lower and upper edges of the cell in the image. The length of the cell is then taken to be the difference between the 2 points and the position of the cell is estimated as the average between the 2 points. The values are then normalized by dividing by the cantilever length in pixels.

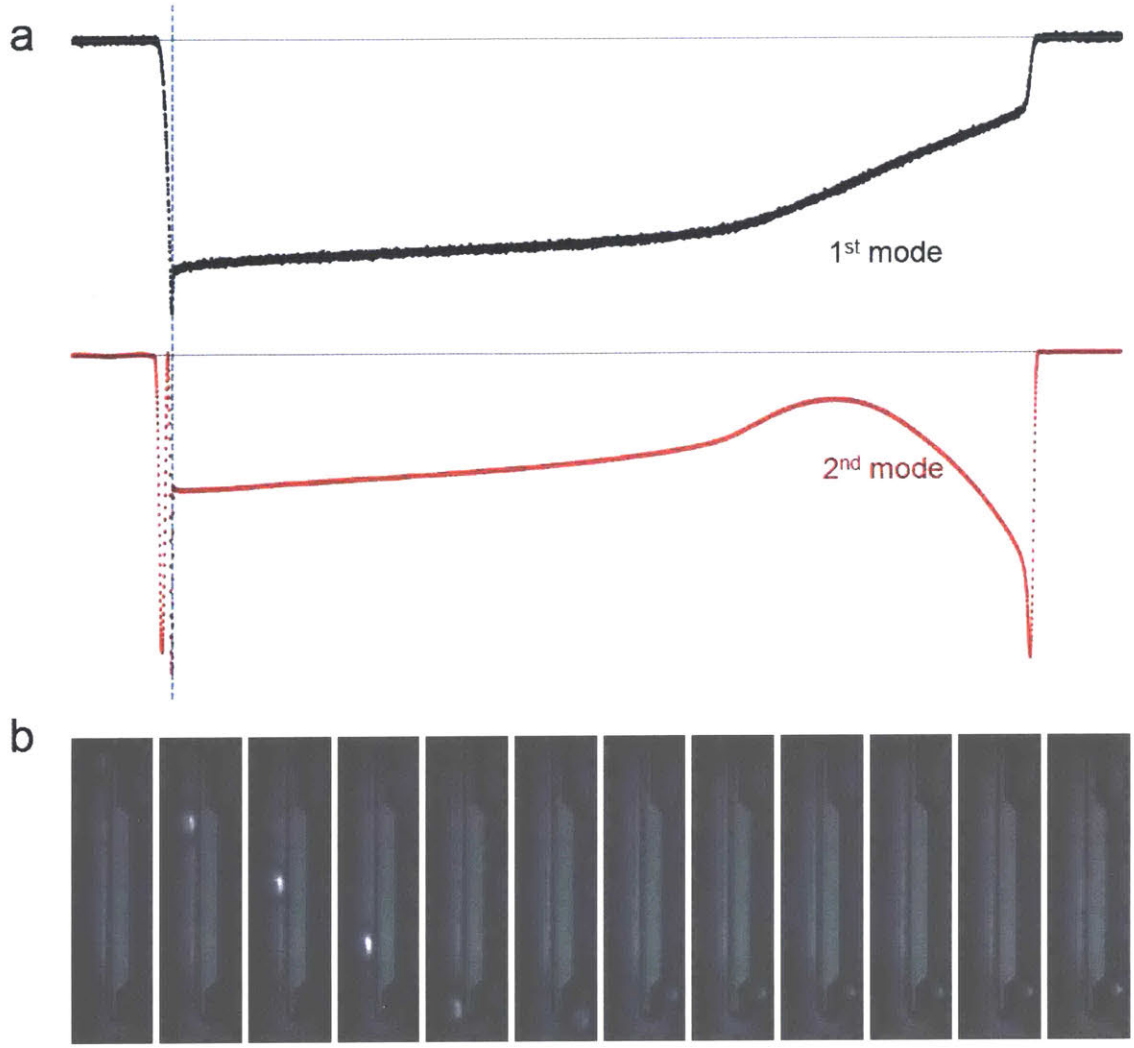

Figure 5-4: Alignment between modes
(a) Alignment of first and second mode peaks using the main peaks of each mode where the cell is at the tip of the cantilever. The dotted line highlights the alignment of this part of the peak in both modes. (b) Example time-series of a U2OS cell entering a constriction. Time between frames is approximately 6.7 ms (frame rate is set at 150 fps).

5.5 Fine alignment of image and frequency data

The frequency signals from the first and second resonant modes can aligned by time-shifting one of the signals such that the first mode peak lines up with the main peak in second mode, as shown in **Figure 5-4**. (The second mode peak has 3 peaks: 1 main peak and 2 side peaks which occur as the cell crosses the antinode during entry and exit.) This works because these points on the respective resonant mode signals correspond to the time at which the cell passes the tip of the cantilever. Alignment of the two frequency signals is accurate to within the frequency acquisition rate. This alignment step needs to be performed only once for each experiment, unless there is some loss of frequency data in one or both modes during data-transfer from the FPGA to the computer leading to a change in alignment of the respective mode signals in the middle of an experiment.

Correctly aligning the frequency and image data is more challenging. After receiving signals from the photodetector or piezo-resistor, the FPGA sends frequency information to the computer in packets of 128 frequency data-points. This corresponds to an uncertainty of 64 ms at a 2000 Hz acquisition rate. In comparison, the time taken for a cell to fully transit the cantilever is on the order of 100 ms to 1 s. Therefore using just the trigger timings outlined in the previous section for alignment of the signals can lead to significant misalignment of frequency and image data leading to large errors in mass estimation. Hence, a second fine alignment step is required to obtain accurate estimates of mass corresponding to each measured image.

To do this, we make use of the first section of the peak in which the cell moves from the base to the tip of the cantilever prior to its entry into the constriction. During this phase the cell is relatively spherical and fully suspended in fluid, hence we do not expect any change in mass. We assume a fixed mass for the cell over this section of the peak and model the cell as a point mass. (The cell can also be modeled as a uniform distribution, but this does not significantly affect results). Making these assumptions, we can find the time-shift between image data and the frequency data that minimizes the sum of the squares of the error between the masses calculated at each image frame. In other words, given a vector of cell positions, and vectors of frequency values for the 2 modes, we find a global best estimate for both time-shift (t_{shift}) and cell mass (Δm):

$$\chi^2\left(\vec{z}, \frac{\Delta m}{m_0}, s\right) = \sum^{F}\sum_{n=1}^{N} \frac{1}{\sigma_n^2}\left(\frac{\omega_{\Delta m,n}(\vec{t} + t_{shift})}{\omega_n} - \frac{s_n}{\sqrt{1 + \frac{\Delta m}{m_0} U_n^2(\vec{z})}}\right)$$

This time-shift is then used as the optimal alignment between signals for the section of the peak where the cell is in the constriction, and mass is not assumed to be constant. Once the time-shift is used to align the frequency data with each image frame, the cell mass corresponding to each image frame is estimated using the position values from the image and the first and second mode frequency values.

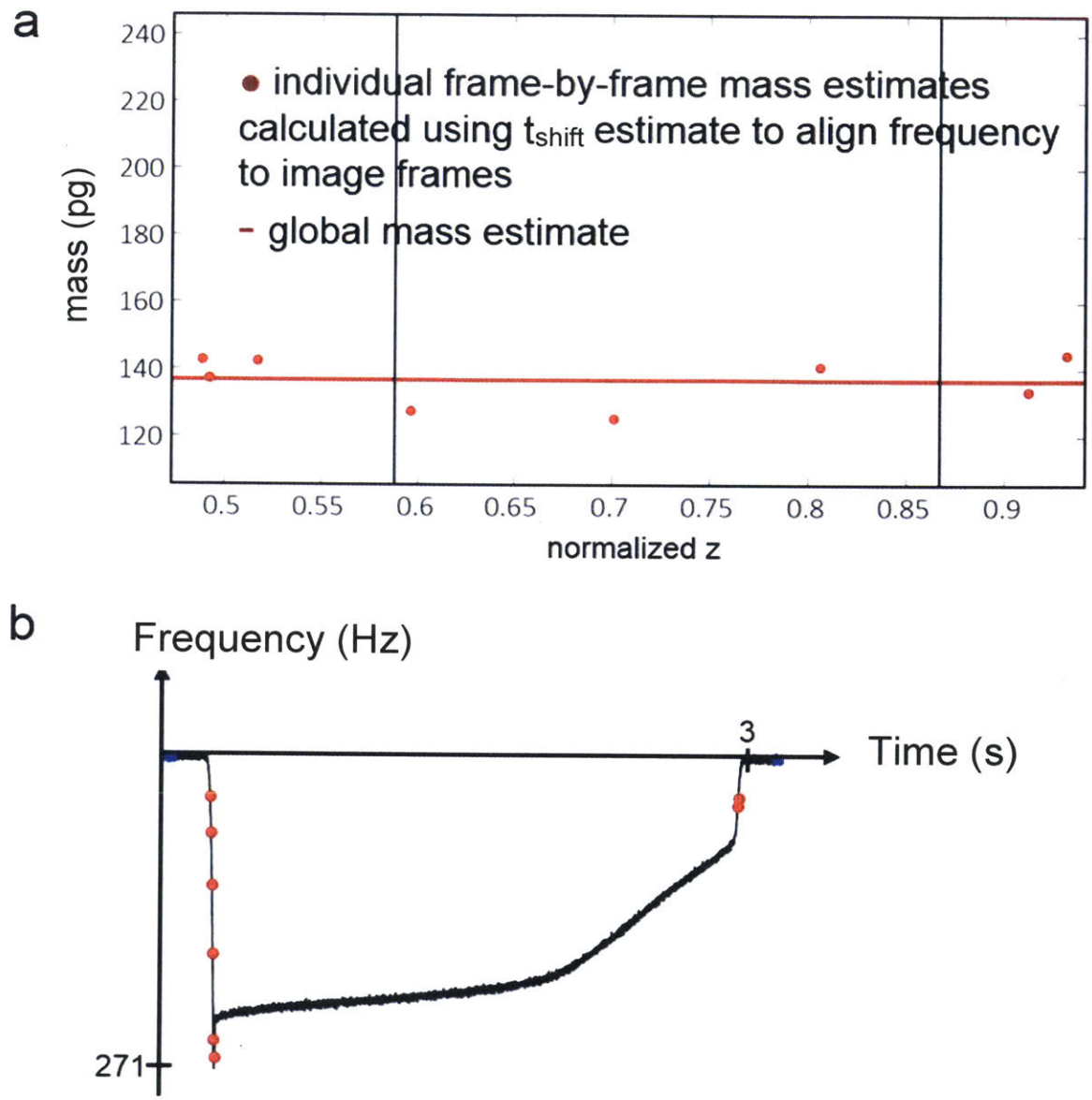

Figure 5-5: Estimation of mass pre-constriction and time alignment
(a) Global mass estimate compared to mass estimates from individual frames for a representative cell. (b) An alternate graphical representation to check for accuracy of the global estimate: a plot of frequency estimates using the global mass estimate and position data from each image frame, superimposed on the actual frequency signal in first mode. Data is aligned using the global time-shift estimate.

5.6 Results of mass estimation

We measured an adherent cell line (U2OS) and a suspended lymphoid cell line (L1210) in a 350 μm long cantilever with a 5 x 15 x 50 μm constriction using the method outlined above. A representative measurement of a typical U2OS cell is shown in **Figure 5-6**. A typical U2OS cell has a mass in the approximate range of 50 – 150 pg. L1210 cells are not shown but exhibit similar patterns of estimated mass changes with much smaller magnitude due to the smaller size of the cells (~30 – 90 pg and 10μm in diameter) resulting in less deformation of each cell when passing through the constriction.

We observed that the estimated masses calculated using our aligned position and frequency data showed very large increases as the cell first enters the constriction, followed by a second peak in estimated mass before the cell mass drops back to the original mass of the cell before entering the constriction. However, the mass changes observed can be as large as 50% of the total mass of a cell. Since it is unlikely that the cell density can change by such a large amount just due to water exiting the cell membrane, we suspected that the mass estimates may be erroneous.

For entry into the cantilever, we do expect some estimation error due to the complex shape of the cell, where a small portion of the cell is stuck the constriction and a larger section is just outside the constriction. Since our model assumes a uniform cell mass distribution and does not account for shape changes, we expect some measurement

artifacts just at the entry of the constriction. However, the apparent mass continues to rise even when the cell has fully entered the constriction and has a more regular oval or pill-like shape. In addition, the second large increase in apparent mass in the middle of the constriction is difficult to explain. It is possible that a cell reabsorbing water may decrease in buoyant mass, but a change of as much as 20% of the cell's mass in less than 1s is unlikely to be explained by such a mechanism.

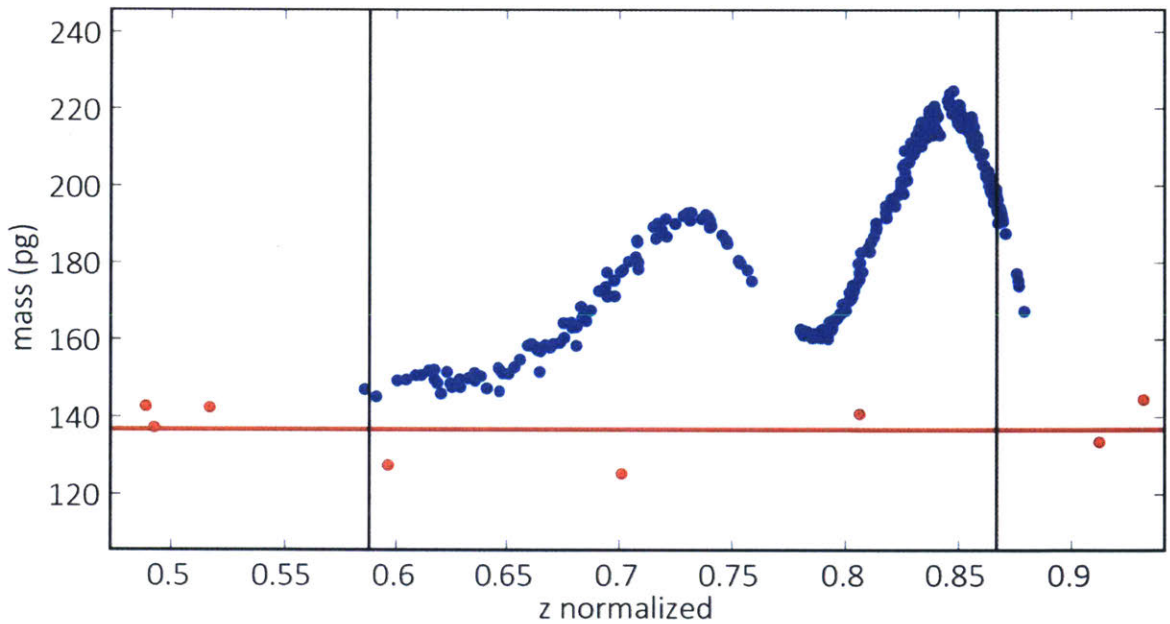

Figure 5-6: Typical mass estimate of U2OS cell
Mass estimates of a typical U2OS cell passing through a cantilever with constriction. Blue dots show the mass estimates for each image frame while the cell is passing though the constriction. As in **Figure 5-5**, the red line shows the global mass estimate and red dots show the mass estimation error for frames prior to entry into the constriction. Black vertical lines denote the start and end of the constriction in normalized position along the length of the cantilever.

To further analyze this result, we decided to instead represent the data as the difference between the measured frequency and the frequency that would be expected if the cell did not change in mass. This idea is illustrated in **Figure 5-7** which plots the raw frequency data from prior to entry into the constriction with the frequency data during transit though the constriction. In the figure, the frequency is interpolated to position to better visualize the difference in frequency at identical positions along the length of the cantilever. One can see that the frequency is lower in the constriction than outside it. This frequency change would be a combination of a change in mass and any other factor that affects the frequency measurement.

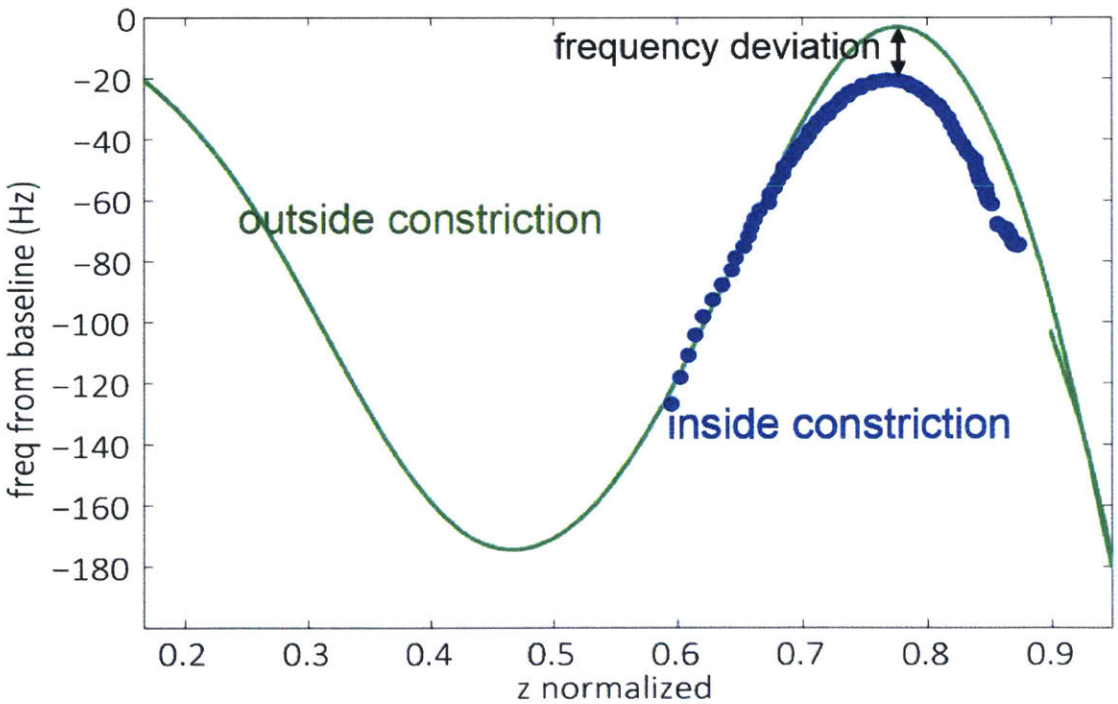

Figure 5-7: Frequency deviation shown as a function of position
Plot of peak frequency as a function of position comparing frequency data outside the constriction to frequency data from inside the constriction

When this frequency is plotted (see **Figure 5-8**) we find that there is an almost linear variation in frequency deviation increasing in a base-to-tip direction along the length of the cantilever. This suggests that the fluctuation in mass estimation is an artifact of this linearly changing frequency deviation. This linear deviation causes an error in mass estimation that varies with the mode-shape in the second resonant mode.

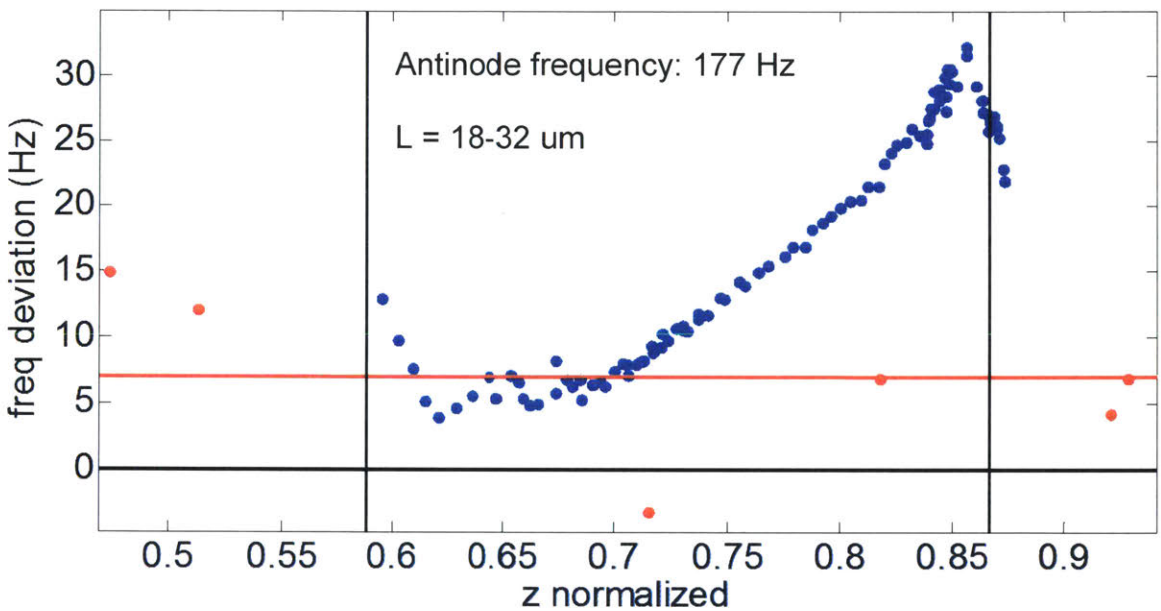

Figure 5-8: Representative plot of frequency deviation in a U2OS cell.
The blue plot shows deviation in frequency (in Hz) from a peak with antinode height of 177 Hz from the expected frequency if the cell does not change in mass. The red line and dots show masses calculated from image frames outside the constriction, as in the previous figures.

5.7 Possible causes of erroneous mass estimate

Our technique for fine-alignment of image frames to frequency provides a series of cell-mass estimates in positions where the cell has not yet entered the constriction and is not changing in mass. This gives some confidence that the alignment is reasonably accurate since the estimates have an uncertainty of up to at most 10% of cell mass (see distribution of red dots in **Figure 5-5**). Hence we suspect that some kind of frequency change independent of mass may be responsible for the unusual mass estimates.

One possibility for such a mass-independent frequency change is cell interaction with an acoustic standing wave in the cantilever. Mass estimation in this technique (as well as in previous sections) neglected any interaction between the cell and surrounding fluid and assumed local fluid kinetics to be unaffected by the presence of a cell immersed in fluid. The effect of acoustic-cell interactions on the total kinetics of a fluid-cantilever system is usually minimal and results in only a small deviation in frequency. We suspect that this effect could be significantly amplified as a cell passes through the constriction because the cell completely occupies the narrow space, acting as a physical barrier blocking the fluid column. However, our current understanding of this cell-fluid interaction in the constriction is limited and we were unable to quantify its effect. Another possibility for the mass-independent frequency shift is the interaction between the cell and the wall of the constriction. The physical contact may result in a local change of the effective spring constant of the cantilever, altering the resonant frequency.

5.8 Conclusion

In conclusion, we have developed a technique for performing simultaneous measurement of resonant frequency and cell position in a suspended cantilever, including the necessary post-processing for synchronization and mass estimation. However, we observed a much larger than expected mass shift, which is not fully understood but may be related to cell-fluid interactions creating a mass-independent frequency shift.

Hence, although there are no technical barriers to implementing this technique, the presence of mass-independent frequency deviations means that the desired measurement of single-cell mass changes due to change in water content of the cell cannot be measured in this way. This technique for mass estimation should be avoided especially for cases when (a) the mass change is small and (b) the expected change in mass occurs simultaneously with position changes along the length of the cantilever.

Chapter 6

Towards measurement of mass accumulation in adherent mammalian cells

6.1 Introduction

So far, all MAR measurements in the previous chapters have involved suspended cells. It has been shown both in this thesis and other work that very high precision can be obtained in suspended cell measurements. Suspended cell MAR measurements are ideal for cell lines that grow natively as suspended single cells, such as hematopoietic or lymphoid cell lines and tumor isolates. It can also be more broadly applied to short term measurements of single cells dissociated from clumps of cells (as shown with GBM cells in the first part of this thesis) or to cells detached from a culture surface.

However, such measurements are limited in time since the cells will eventually revert from a single cell state to its preferred culture configuration. In addition, we cannot be certain that cells that natively grow in adherent culture will accumulate mass at the same rate or grow with the same proliferation dynamics when removed from the culture surface and measured in the form of suspended single cells.

In both basic biology and cancer research, a large majority of the existing cell lines used as models grow while adhered to the surface of a culture flask. Hence it would be beneficial if we could extend the MAR measurement to making direct measurements on such adherent cells, measuring the cells while they are adhered to channels within an SMR. In this chapter we will describe the steps we took to adapt the MAR measurement for this purpose, by using the system described in the last chapter to combine image and frequency data, and by using a second reference cantilever to make a differential measurement that helps to account for frequency drift.

6.2 Suspended particle measurements vs adherent measurements in an SMR

When the SMR was first developed, the authors [2] envisioned its use in two alternate ways. First, as a molecular binding assay in which particles bind to the inner surface of the channel within the cantilever, and second, as a particulate mass measurement, utilizing the frequency deviation caused by a suspended particle passing through the cantilever's channel. Since this first demonstration almost all applications of the SMR have involved particulate measurements, suggesting such a mode of measurement as ideally suited to SMRs.

Due to the nature of particulate measurements, both position uncertainty and frequency drift can be almost completely eliminated. Conversely, making measurements of any particles bound or adhered to the cantilever channel is inherently more difficult due to these factors. However, improvement in measurement techniques related to the SMR over the last few years may open up the possibility of measuring adherent cells reliably. In the next section we outline the main obstacles to measuring viable adherent cells in an SMR, show how such problems are comparatively less relevant in suspended cell measurements, and explain how we can overcome these issues to begin to make adherent cell measurements.

6.3 Overcoming engineering challenges inherent to measuring adherent cells

6.3.a Cell position uncertainty

In suspended cell measurements, position uncertainty is not an issue since during every measurement a cell must pass through antinode of the second resonant mode, during which a frequency minimum is observed. Hence we can make extremely consistent measurements utilizing this well-defined position by finding the value of this frequency minimum relative to the baseline frequency. However, in the case of adherent cells, the cells remain in the cantilever and have the ability to crawl along the length of the channel. Since the mass sensitivity in both the first and second resonant modes varies significantly with position along the cantilever, it is critical to know the position of the cell in order to parse the frequency measurement into a mass estimate.

In addition to requiring knowledge of the position of the cells, adherent cells have a tendency to stretch out over 10s of microns along a culture surface, making it necessary to account for the length of the cell along the long axis of the cantilever. We obtain information on both position and extent of the cells using the same infrared camera used in chapter 6, and make use of a simple uniform mass distribution model described on page 81.

6.3.b Maintaining cell viability

The procedures for maintaining cell viability in suspended cells have been described in detail in earlier chapters. We continue to utilize these adaptations in adherent cell measurements, particularly the control of chip temperature at 37°C and pressurization of all fluid vials with 5% CO_2 to mimic conditions in a cell culture incubator. Unlike in suspended cells which spend the majority of their time in the bypass channels and only a small fraction of their time in the resonator, adherent cells remain in the resonator at all times.

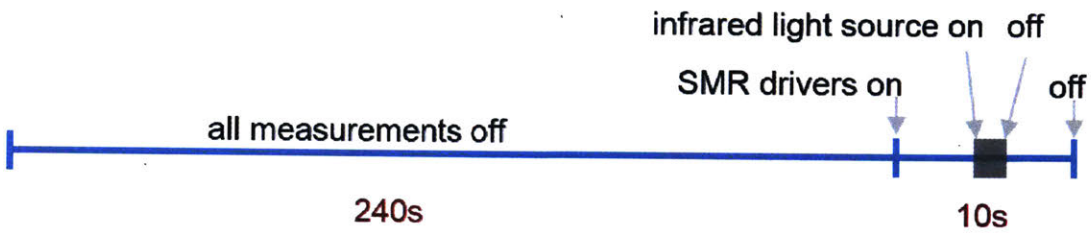

Figure 6-1: Measurement cycle illustration
Schematic of a single cycle of measurement involving short periods of frequency measurement and infrared light source activation followed by image capture. (Lengths not to scale)

To ensure that the cell is not perturbed excessively by both the frequency and image measurements, we explicitly control the duty cycle in which both frequency and imaging measurements are taken (**Figure 6-1**). To do this, we set up a Labview program to perform a repeated fixed sequence in which all measurements are turned off for a fixed time (4-5 min), followed by a short period (up to 10s) of frequency measurement. This frequency measurement is bisected by a 200ms window during which the infrared light source is turned on and images are captured and saved.

The duty cycle can be tweaked to either increase the frequency of measurement if higher acquisition rates are desired or decreased to allow for growth of more sensitive cells.

6.3.c Frequency drift

The main benefit of suspended cell or particle measurements is the relative unimportance of frequency drift, since the cell transits the cantilever in less than half a second during which little to no frequency drift has occurred. In comparison, for an adherent cell measurement, since the cell remains in the cantilever throughout the measurement it is impossible to interrogate the frequency of the cantilever absent the cell while the cell is being measured. Due to frequency drift, the frequency measured before the cell is loaded into the cantilever may not be the correct reference frequency for use at a later time.

To compensate for this frequency drift, the most practical solution is to perform a differential measurement. In our application we utilize a multi-cantilever chip (**Figure 6-2**) to make a reference measurement using a second cantilever that is fluidically connected to the main cantilever containing the cell. The frequency changes measured in the second cantilever can be used as a proxy for frequency drift in the main cantilever, enabling us to estimate what the frequency of the main cantilever would be without a cell in it.

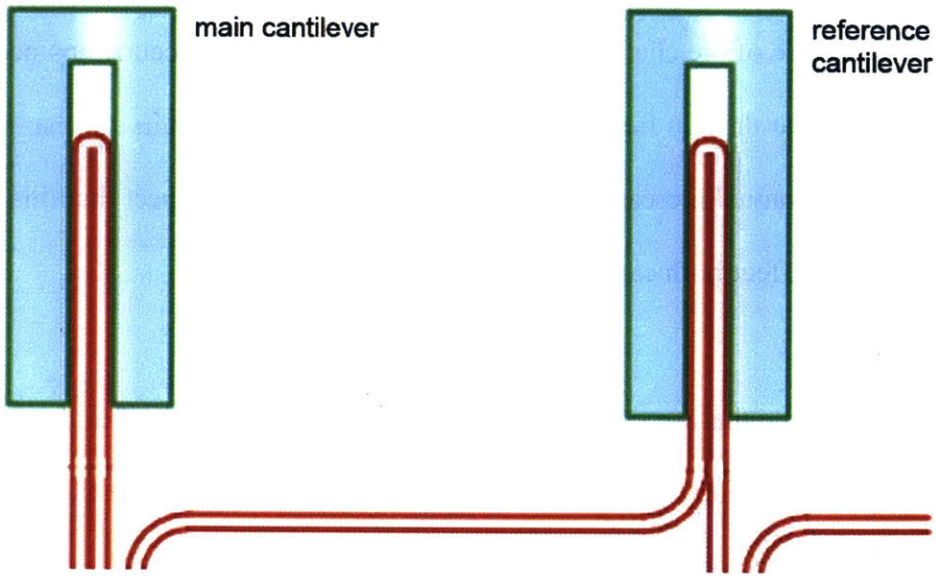

Figure 6-2: Multi-cantilever chip design repurposed for reference measurement
Shown here is the relevant section of the chip design showing a second cantilever for reference measurement. The cantilevers are fluidically connected by an adjoining channel. The full chip contains 12 cantilevers but only the first 2 are being used. Original chip design is by Robert Kimmerling and is design 707 in the 7th generation of wafers fabricated by LETI.

Although frequency drift in a SMR is difficult to characterize, there are a number of sources of frequency drift that we are aware of. These include (1) the temperature of the resonator, (2) the vacuum pressure in the vacuum cavity surrounding the resonator, (3) the pressure of the fluid contained within the resonator, and (4) the local density of the media within the cantilever. The temperature and pressure of the vacuum cavity (points 1-2) are relatively uniform over all cantilevers on the chip. Assuming that there is some flow between channels of the 2 cantilevers, both density and pressure of fluid with the channels (points 3-4) will be almost identical over the 2 cantilevers.

In addition, one possible source of frequency drift is the build-up of proteins from the media on the surface of the channels. We hypothesize that this is occurring since we often observe a near-linear drop in frequency only when media is present in the channels, which suggests a gradual increase in mass of the cantilever. We expect that this phenomenon will affect both cantilevers in a similar manner.

It is important to note that we do not know the relative contributions of each of the above factors to the final measurement, nor do we fully understand all the factors that result in drift. However, any factor that affects both cantilevers equally will be eliminated by the reference measurement. Although we aim to eliminate most of the drift in this manner, there will still be some sources of drift which may affect the two cantilevers differently, causing them to drift relative to each other.

We performed a test of reference measurements illustrated in **Figure 6-3**. The chip was loaded with conditioned DMEM media isolated from Hela cells grown for 3 days. (This is the same media that we use to culture the cells on-chip.) The measurement was taken for 80 hours, showing that the drift can be reduced by an order of magnitude from 40 Hz to approximately 4 Hz over this time period in the second resonant mode. However, similar measurements in the first mode showed only a small reduction in drift, of approximately a factor of 2 (**Figure 6-4**).

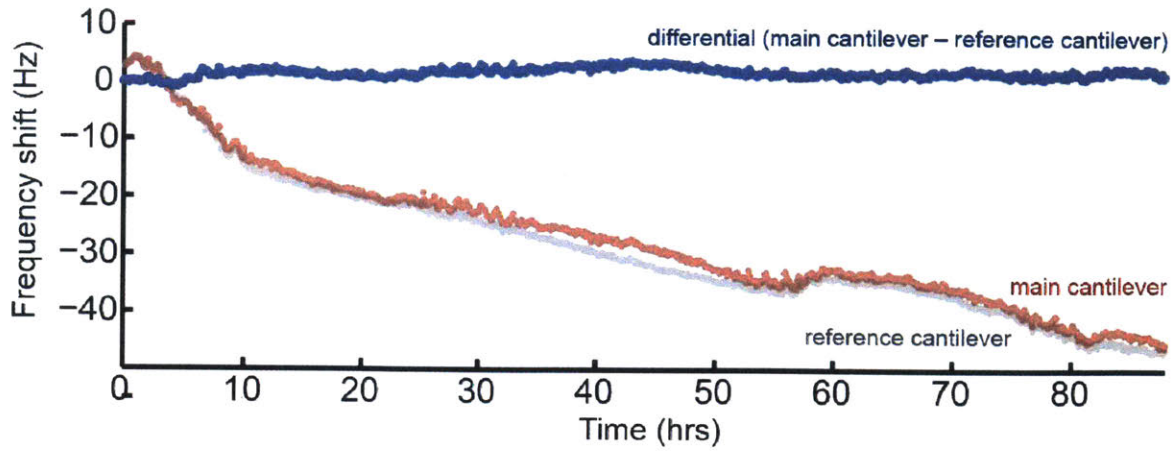

Figure 6-3: Differential measurement in second resonant mode
Example of a differential measurement in the second resonant mode with only conditioned DMEM media pressurized on all entry ports with 5% CO_2 at 4psi. Each datapoint shown is the average of the frequency data in 1 measurement cycle. We used the first 2 cantilevers on the chip (707 design), which are separated only by a short channel distance (~1500um) and a hydrodynamic trap. The frequency shift is shown relative to the resonant frequency of the cantilever measured at the start of the experiment.

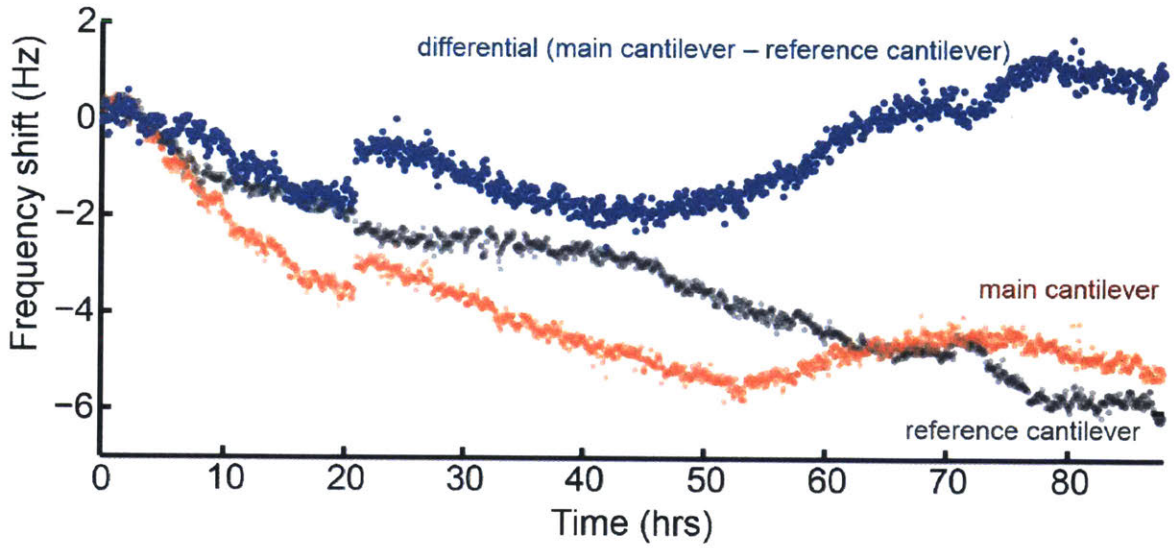

Figure 6-4: **Differential measurement in first resonant mode**
Example of a differential measurement in the first resonant mode with same conditions as the previous figure. Note that the relative drift between the cantilevers is much larger compared to its sensitivity in this mode (a few Hz at the typical position of the cell).

6.4 Results and discussion

We measured a Hela cell for approximately 2 generations witnessing 2 sets of cell divisions. The raw data for the measurement including both reference frequency and differential measurement are shown in **Figure 6-5**.

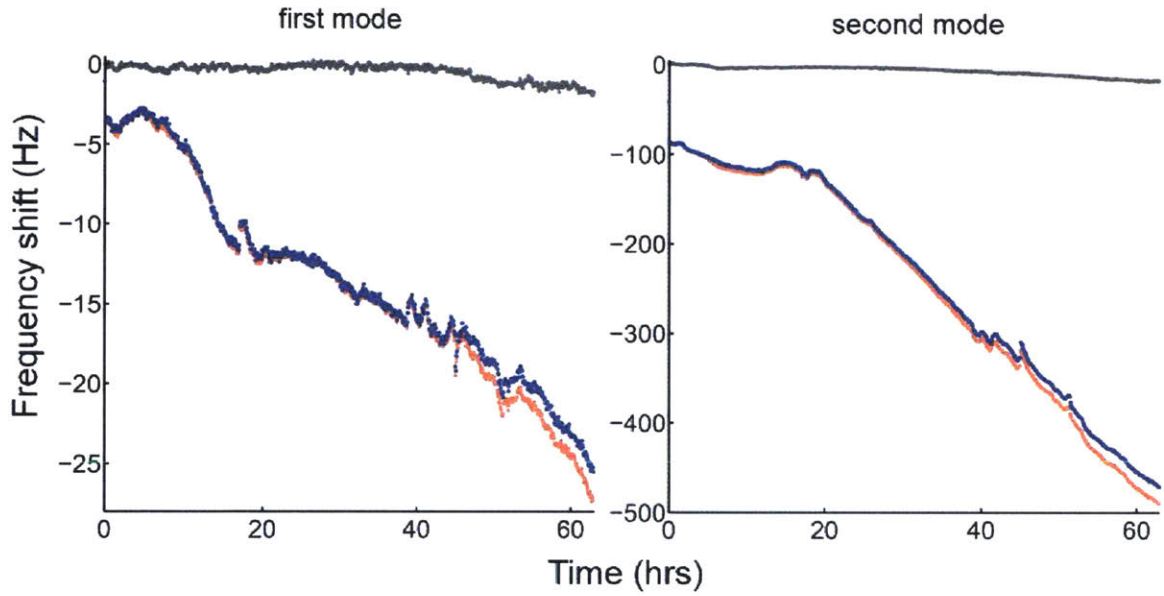

Figure 6-5: Raw data from measurement of Hela cell over 2 generations
The figure shows the raw data in both first and second resonant modes from the main cantilever containing the cell (red) and the reference cantilever holding only media. The line in blue shows the differential measurement.

The mass estimate combining frequency and image data is shown in **Figure 6-6**. We observed that after 1 hour of almost no mass accumulation, the mass of the cell increased monotonically during most of the cell cycle. The original slow mass accumulation may be related to acclimation of the cell to its environment or may reflect the process of adhering fully to the channel surface.

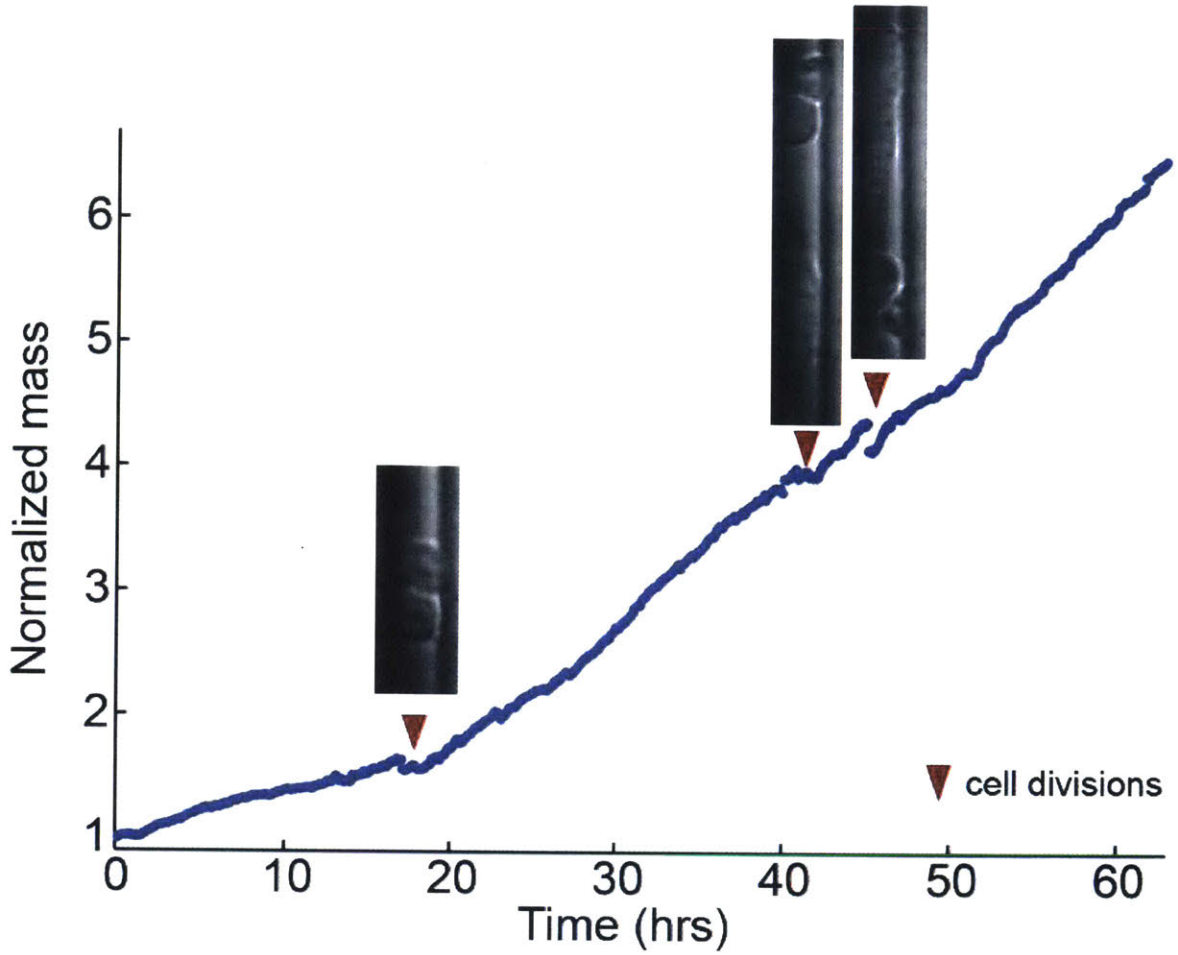

Figure 6-6: Mass estimate of Hela cell grown for 2 generations
The plot shows the mass estimates relative to the original mass of the cell when loaded. Cell divisions (both original and both daughter cells) are shown by red arrows, and pictures of the cells at those points are included. According to typical sensitivities of similar chip designs, the starting mass of the cell is approximately 110 pg.

During time periods close to cell division, mass accumulation appears to slow down. However, it is unclear if the change in cell shape or attachment of the cell to the channel wall is affecting the measurement at this point since the cell detaches slightly from the channel walls and forms up into a ball before cytokinesis.

6.5 Future directions

Significant further refinement will be required to make measurements of adherent cells accurate enough for study of cell cycle dynamics. In terms of data processing, more accurate models could be used. For example we can use separate uniform mass distributions for each cell in cases of 2 or more cells. This would be an improvement over the crude estimate of a uniform distribution stretching over multiple cells. We can also make further improvements by using more complex mass-distributions to model the outline of the cell observed in the image and project the area of such an outline onto the long axis of the cantilever.

One significant improvement that can be made while keeping the existing chip design is to measure the third resonant mode of the cantilever. The main benefit of measuring this mode is the ability to compensate for the low sensitivity at the second mode node, where sensitivity is close to zero in the second mode but very high in the third mode. The combination of second and third modes will allow for accurate measurements to be made at any point along the channel regardless of where the cell crawls, as long as it does not leave the cantilever. In addition, combining two highly sensitive modes opens up the possibility to resolve the masses of 2 cells at separate locations along the length of the cantilever, such as daughter cells that have migrated away from each other but remain in the cantilever channel.

In terms of chip design, a number of tweaks can be made to achieve better correlation between the main and reference cantilevers. The main design modification would be to move the 2 cantilevers closer together and reduce the amount of channel between them. This would reduce local fluid density differences between the 2 cantilevers, and further reduce the effects of local variations in temperature. In addition, the cantilever channel should extend to the tip of the cantilever to allow for maximum sensitivity in the first mode. An example of such a design is shown in **Figure 6-7**.

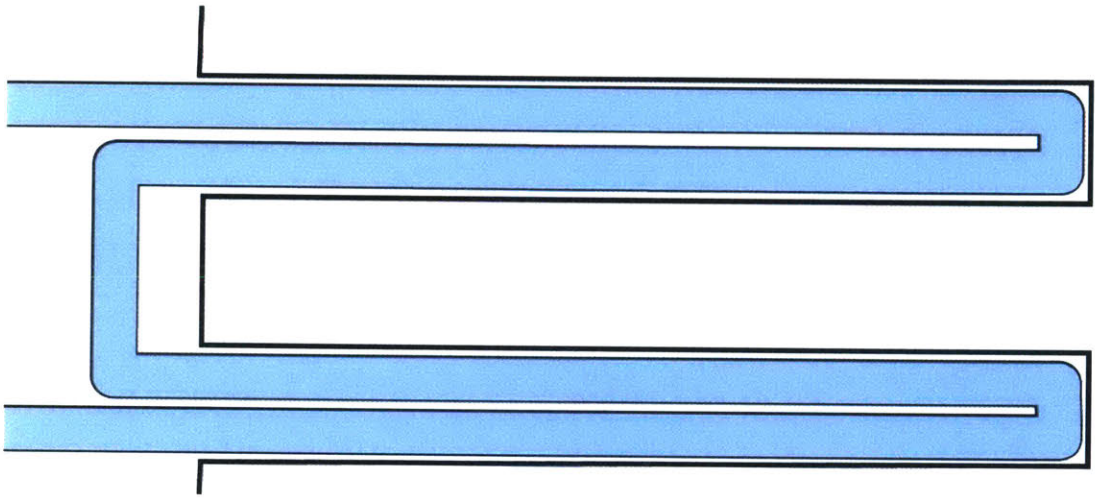

Figure 6-7 Tweaks in chip design for improved adherent cell measurement
Cantilevers can be placed as close together as possible while allowing space for piezoresistor leads. There should be minimal intervening channel between the cantilevers, and channels should extend to the tip of the cantilever.

6.6 Conclusion

In conclusion, we have shown the first measurements of adherent cells in SMRs, and explained how a number of adaptations and engineering solutions were required to achieve such a measurement. Much work still has to be done to refine the measurement, and we expect that in future it may be possible to achieve sufficient precision to reveal insights into cell cycle dynamics as well as provide the ability to detect perturbations on the cell ranging from drug effects to nutrient deprivation.

6.7 Appendix 1: Alternate mass trajectory data

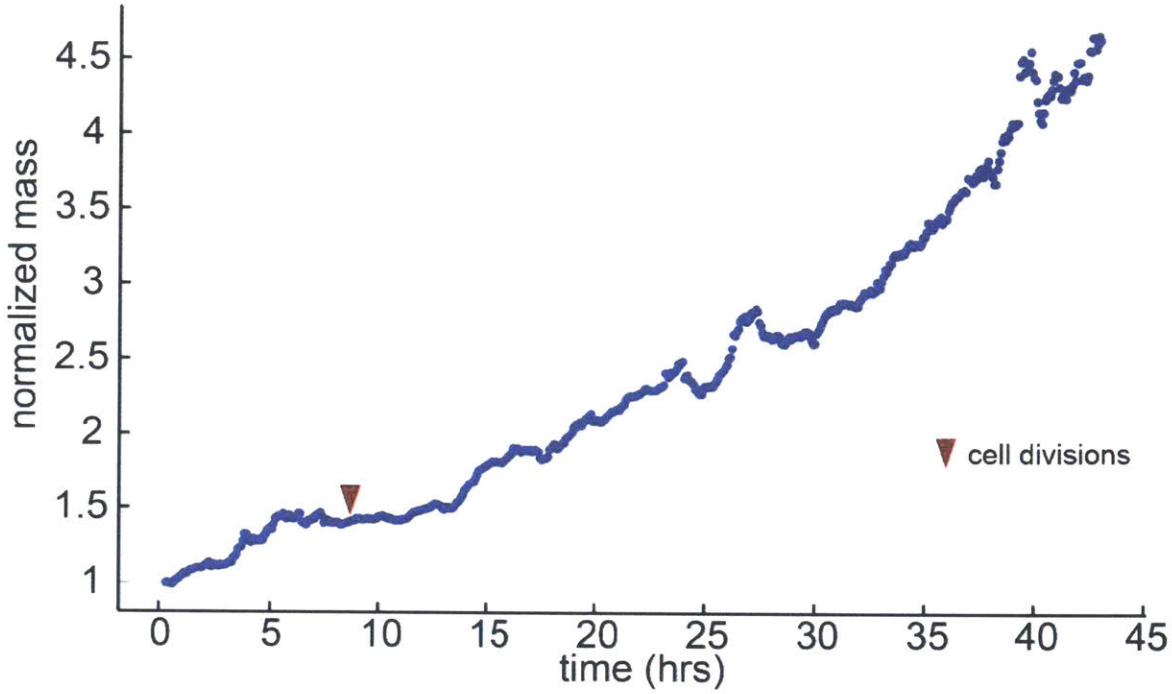

Figure 6-8: Alternative mass estimate trajectory for a cell
An alternative mass trajectory of a different cell that was measured. Note that in this measurement there was a second cell growing in nearby channels outside the cantilever. Approximate mass of this cell is 150 pg.

6.8 Appendix 2: Frequency noise compared to drift over time

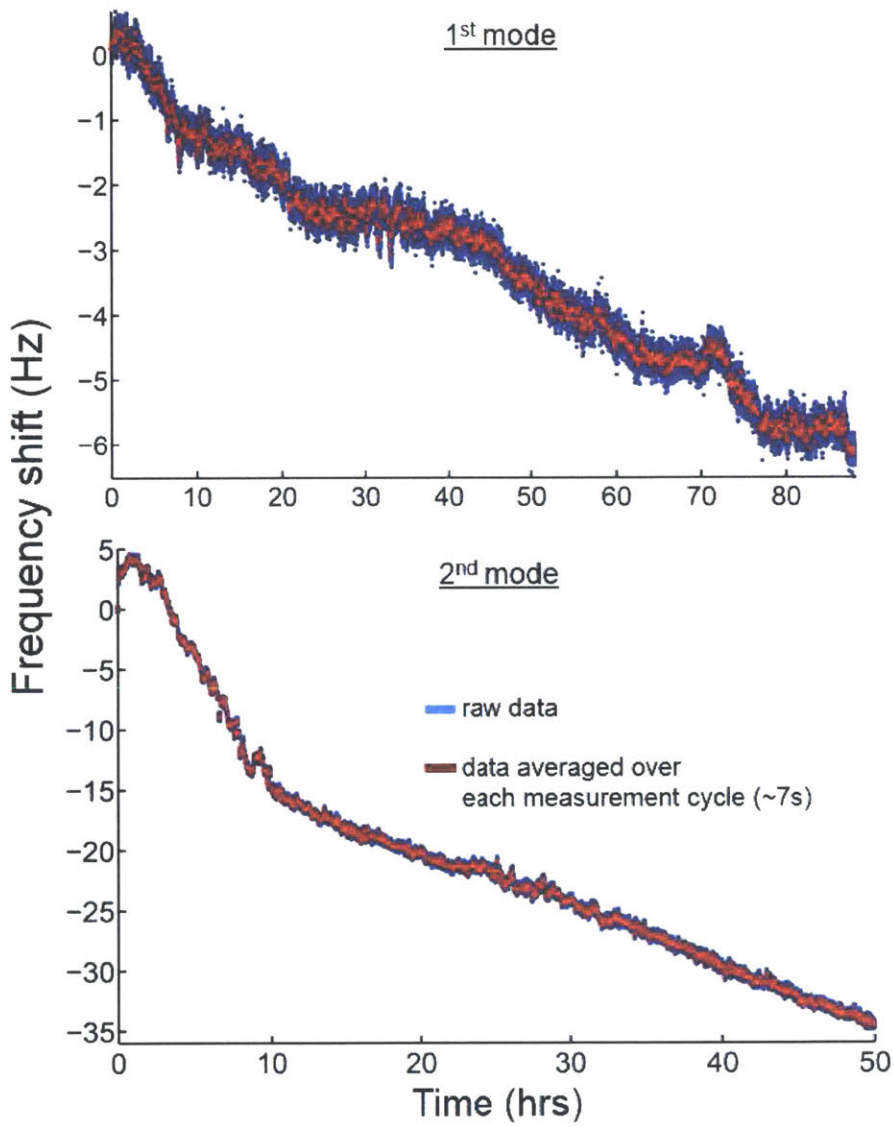

Figure 6-9: Frequency noise vs long term drift
Plot of frequency data (blue) and frequency data averaged over each cycle (red) for 2 modes with DMEM media fully pressurized with 5% CO_2 in the cantilever over a period exceeding 50 hrs. 2nd mode data is shown over a shorter time due to much greater frequency drift. The data shows that drift is much more significant than measurement noise over long periods on the order of days.

6.9 Appendix 3: Manual identification of cell boundaries

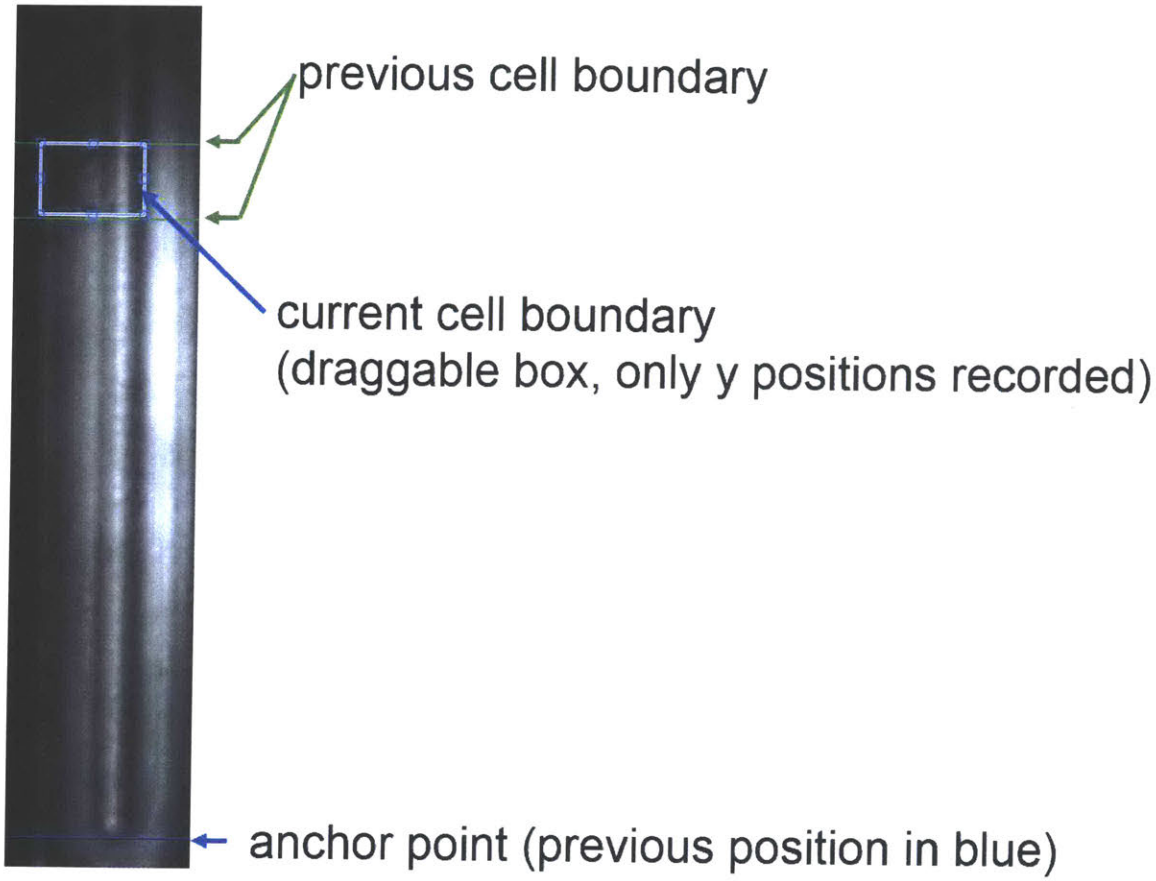

Figure 6-10: Procedure for drawing cell boundaries in matlab code
Before starting the analysis, the user can select a region of interest (ROI) so that only the cantilever area is seen. For each measurement cycle, all images taken are averaged and presented as an image in matlab, shown in the figure. The user can then select the anchor point, which is the end of the inner channel wall near the tip. Press enter after done. If nothing is selected, the code defaults to the anchor point from the previous cycle. The user can then choose the cell boundary by a draggable box (using matlab function imrect), double-clicking when done.
The y values of the boundary are recorded and converted to a cell position and length. From these values, the distances in pixels from the anchor point is calculated for the center of the cell, converted to um and subtracted from the known length of the anchor point from the base of the cantilever. The normalized cell position is then calculated by dividing this distance (in um) from the total length of the cantilever (in um). The cell length is similarly calculated by converting the pixel value to um and dividing by length of the cantilever.

Bibliography

1. Datar R, Kim S, Jeon S, Hesketh P, Manalis S, Boisen A, Thundat T: **Cantilever Sensors: Nanomechanical Tools for Diagnostics.** *Mrs Bulletin* 2009, **34:**449-454.
2. Burg TP, Godin M, Knudsen SM, Shen W, Carlson G, Foster JS, Babcock K, Manalis SR: **Weighing of biomolecules, single cells and single nanoparticles in fluid.** *Nature* 2007, **446:**1066-1069.
3. Burg TP, Mirza AR, Milovic N, Tsau CH, Popescu GA, Foster JS, Manalis SR: **Vacuum-packaged suspended microchannel resonant mass sensor for biomolecular detection.** *Journal of Microelectromechanical Systems* 2006, **15:**1466-1476.
4. Montero J, Sarosiek KA, DeAngelo JD, Maertens O, Ryan J, Ercan D, Piao HY, Horowitz NS, Berkowitz RS, Matulonis U, et al: **Drug-Induced Death Signaling Strategy Rapidly Predicts Cancer Response to Chemotherapy.** *Cell* 2015, **160:**977-989.
5. Bryan AK, Goranov A, Amon A, Manalis SR: **Measurement of mass, density, and volume during the cell cycle of yeast.** *Proceedings of the National Academy of Sciences of the United States of America* 2010, **107:**999-1004.
6. Son S, Tzur A, Weng Y, Jorgensen P, Kim J, Kirschner MW, Manalis SR: **Direct observation of mammalian cell growth and size regulation.** *Nature Methods* 2012, **9:**910-+.
7. Crystal AS, Shaw AT, Sequist LV, Friboulet L, Niederst MJ, Lockerman EL, Frias RL, Gainor JF, Amzallag A, Greninger P, et al: **Patient-derived models of acquired resistance can identify effective drug combinations for cancer.** *Science* 2014, **346:**1480-1486.
8. Lee J, Bryan AK, Manalis SR: **High precision particle mass sensing using microchannel resonators in the second vibration mode.** *Review of Scientific Instruments* 2011, **82**.

9. Johnson DR, O'Neill BP: **Glioblastoma survival in the United States before and during the temozolomide era.** *Journal of Neuro-Oncology* 2012, **107:**359-364.
10. Wen PY, Kesari S: **Malignant Gliomas in Adults.** *New England Journal of Medicine* 2008, **359:**492-507.
11. Stupp R, Mason WP, van den Bent MJ, Weller M, Fisher B, Taphoorn MJB, Belanger K, Brandes AA, Marosi C, Bogdahn U, et al: **Radiotherapy plus Concomitant and Adjuvant Temozolomide for Glioblastoma.** *New England Journal of Medicine* 2005, **352:**987-996.
12. Hegi ME, Diserens A-C, Gorlia T, Hamou M-F, de Tribolet N, Weller M, Kros JM, Hainfellner JA, Mason W, Mariani L, et al: **MGMT Gene Silencing and Benefit from Temozolomide in Glioblastoma.** *New England Journal of Medicine* 2005, **352:**997-1003.
13. Chin L, Meyerson M, Aldape K, Bigner D, Mikkelsen T, VandenBerg S, Kahn A, Penny R, Ferguson ML, Gerhard DS, et al: **Comprehensive genomic characterization defines human glioblastoma genes and core pathways.** *Nature* 2008, **455:**1061-1068.
14. Karsy M, Neil JA, Guan J, Mahan MA, Colman H, Jensen RL: **A practical review of prognostic correlations of molecular biomarkers in glioblastoma (vol 38, E4, 2015).** *Neurosurgical Focus* 2015, **38**.
15. Verhaak RGW, Hoadley KA, Purdom E, Wang V, Qi Y, Wilkerson MD, Miller CR, Ding L, Golub T, Mesirov JP, et al: **Integrated Genomic Analysis Identifies Clinically Relevant Subtypes of Glioblastoma Characterized by Abnormalities in PDGFRA, IDH1, EGFR, and NF1.** *Cancer Cell* 2010, **17:**98-110.
16. Kee N, Sivalingam S, Boonstra R, Wojtowicz JM: **The utility of Ki-67 and BrdU as proliferative markers of adult neurogenesis.** *Journal of Neuroscience Methods* 2002, **115:**97-105.
17. Scholzen T, Gerdes J: **The Ki-67 protein: From the known and the unknown.** *Journal of Cellular Physiology* 2000, **182:**311-322.
18. Fujimaki T, Matsutani M, Nakamura O, Asai A, Funada N, Koike M, Segawa H, Aritake K, Fukushima T, Houjo S, et al: **CORRELATION BETWEEN BROMODEOXYURIDINE-LABELING INDEXES AND PATIENT PROGNOSIS IN CEREBRAL ASTROCYTIC TUMORS OF ADULTS.** *Cancer* 1991, **67:**1629-1634.
19. Stevens MM, Maire CL, Chou N, Murakami MA, Knoff DS, Kikuchi Y, Kimmerling RJ, Liu H, Haidar S, Calistri NL, et al: **Drug sensitivity of single cancer cells is predicted by changes in mass accumulation rate.** *Nat Biotech* 2016, **34:**1161-1167.
20. Lathia JD, Gallagher J, Myers JT, Li MZ, Vasanji A, McLendon RE, Hjelmeland AB, Huang AY, Rich JN: **Direct In Vivo Evidence for Tumor Propagation by Glioblastoma Cancer Stem Cells.** *Plos One* 2011, **6**.

21. Deleyrolle LP, Harding A, Cato K, Siebzehnrubl FA, Rahman M, Azari H, Olson S, Gabrielli B, Osborne G, Vescovi A, Reynolds BA: **Evidence for label-retaining tumour-initiating cells in human glioblastoma.** *Brain* 2011, **134:**1331-1343.
22. Verreault M, Schmitt C, Goldwirt L, Pelton K, Haidar S, Levasseur C: **Preclinical Efficacy of the MDM2 Inhibitor RG7112 in MDM2-Amplified and TP53 Wild-type Glioblastomas (vol 22, pg 1185, 2016).** *Clinical Cancer Research* 2016, **22:**2313-2313.
23. Jeay S, Gaulis S, Ferretti S, Bitter H, Ito M, Valat T, Murakami M, Ruetz S, Guthy DA, Rynn C, et al: **A distinct p53 target gene set predicts for response to the selective p53-HDM2 inhibitor NVP-CGM097.** *Elife* 2015, **4**.
24. Andreeff M, Kelly KR, Yee K, Assouline S, Strair R, Popplewell L, Bowen D, Martinelli G, Drummond MW, Vyas P, et al: **Results of the Phase I Trial of RG7112, a Small-Molecule MDM2 Antagonist in Leukemia.** *Clinical Cancer Research* 2016, **22:**868-876.
25. Shalek AK, Satija R, Shuga J, Trombetta JJ, Gennert D, Lu DN, Chen PL, Gertner RS, Gaublomme JT, Yosef N, et al: **Single-cell RNA-seq reveals dynamic paracrine control of cellular variation.** *Nature* 2014, **510:**363-+.
26. Friedman AA, Letai A, Fisher DE, Flaherty KT: **Precision medicine for cancer with next-generation functional diagnostics.** *Nature Reviews Cancer* 2015, **15:**747-756.
27. Jonas O, Landry HM, Fuller JE, Santini JT, Baselga J, Tepper RI, Cima MJ, Langer R: **An implantable microdevice to perform high-throughput in vivo drug sensitivity testing in tumors.** *Science Translational Medicine* 2015, **7**.
28. Yang L, Effler JC, Kutscher BL, Sullivan SE, Robinson DN, Iglesias PA: **Modeling cellular deformations using the level set formalism.** *Bmc Systems Biology* 2008, **2**.
29. Zhou EH, Lim CT, Quek ST: **Finite element simulation of the micropipette aspiration of a living cell undergoing large viscoelastic deformation.** *Mechanics of Advanced Materials and Structures* 2005, **12:**501-512.
30. Dohn S, Svendsen W, Boisen A, Hansen O: **Mass and position determination of attached particles on cantilever based mass sensors.** *Review of Scientific Instruments* 2007, **78**.
31. Olcum S, Cermak N, Wasserman SC, Manalis SR: **High-speed multiple-mode mass-sensing resolves dynamic nanoscale mass distributions.** *Nature Communications* 2015, **6**.